Earl Nick (Orcid ID: 0000-0002-6375-0699)
Simmonds Ian (Orcid ID: 0000-0002-4479-3255)

Sub-synoptic-scale features associated with extreme surface gusts during the South Australia Storm of September 2016 – Part II: Analysis of mechanisms driving the gusts

Nick Earl*[1,2] and Ian Simmonds[1]

[1] School of Earth Sciences, The University of Melbourne, Parkville, Melbourne, Victoria, 3010, Australia.

[2] Institute for Marine and Antarctic Studies, The University of Tasmania, Hobart, Tasmania, 7003, Australia.

*corresponding author – nearl@unimelb.edu.au

Abstract

An extreme extra-tropical cyclone (ETC) struck South Australia on the 28th September 2016, causing state-wide blackouts and damage. In the second part of this two part study, we examine the extreme surface wind producing mechanisms within the ETC. ETCs have been extensively studied in the northern hemisphere (particularly in western Europe), highlighting the gust-producing mesoscale features within. Before now, no southern hemisphere ETC has been examined in this way. There were a number of extreme gust-producing features within the ETC, comparable to those observed in storms over western Europe. These included a convective line, which caused many of the most extreme gusts and knocked out the state power grid. However, dry slot convection also contributed to the extremes and this feature is known to rarely cause extreme gusts in ETCs over the UK, so warrants further analysis to examine whether this is common extreme gust-producing ETC feature over southern Australia. The strongest winds recorded throughout the event

This is the author manuscript accepted for publication and has undergone full peer review but has not been through the copyediting, typesetting, pagination and proofreading process, which may lead to differences between this version and the Version of Record. Please cite this article as doi: 10.1002/wea.3384

occurred on the 29th September, and these were associated with the cold conveyor belt which spiralled around the low-pressure-centre.

Introduction

On the 28th September 2016, an extreme ETC (Extra-tropical cyclone; hereafter ETC28) affected the Australian state of South Australia causing state-wide blackouts and damage. In part 1 of this paper we determined that ETC28 progressed along a common track and followed the Shapiro-Keyser life cycle model often seen in explosive European ETCs. We constructed a track analysis of the event and of similar-tracking ETCs and found that ETC28's low pressure centre deepened more explosively than all but two other ETCs over the past 37 years and reached the lowest central pressure of all. We found that ETC28 potentially contained a sting jet (SJ; Browning 2004); however, if made it to the surface, it was not the cause of the state-wide damage. The ETC centre did not reach landfall until well into stage IV of its life cycle around 0000 UTC on the 29th (Figure 1a) and SJs occur during stages II-III. Here, we focus on the mesoscale features within ETC28 that did cause the most severe surface wind gusts. We also establish whether this Australian ETC exhibited similar features to those seen over western Europe. This is the first southern hemisphere ETC to be split into different sub-synoptic scale features in this way, with its extremity based on surface wind observations.

Features

Within ETCs, there are many mesoscale features which can produce extreme surface winds, and a full description of these features is presented by Earl *et al.* (2017) and in Table S1. Some occur only within explosively deepening ETCs, while others occur in any ETC or (less often) independently. Having established that the extreme winds seen during ETC28 were not associated with a SJ, we explore the other features, which were responsible. Baker (2009) found that extreme surface winds during a UK ETC, Gudrun of January 2005, were associated with the cold conveyor belt (CCB; see Carlson, 1980; Schultz 2001) as it spiralled around the low-pressure-centre on the bent back front and acted in the same direction as the motion of the cyclone (Figure 1b). This was also the case over Germany during windstorm Kyrill in 2007, where there was no SJ identified but intense surface winds occurred in this part of the ETC (Fink et al., 2009). This shows that the CCB can cause high-impact gusts without the presence of a SJ and indeed be the dominant cause of extreme gusts, as Earl *et al.* (2017) concluded using a climatology of UK ETCs. Evidence for both the CCB and SJ causing strong surface winds was presented during the development of UK ETC Ulli (January 2012) by Smart and Browning (2014), and in the broader general discussion of Schultz and Browning (2017). Slater *et al.* (2015) supported this by conducting an idealised study, using the high-resolution Weather Research and Forecasting model to investigate the fine structure of the cloud head and found that separate discrete surface gust maxima during the early stage of frontal fracture.

Earl *et al.* (2017) found convective lines (CLs), comprised of narrow cold frontal rain-bands and post-frontal quasi-linear convective systems, accounted for a third of the strongest 1980-2014 surface gusts observed in the UK. CLs (Figure 1b) are well-known for producing strong winds, including intense downburst winds, a rear inflow jet (Weisman 2001), low-level mesovortices and tornadoes. These systems may produce highly damaging straight-line (non-rotational) winds as part of the rear inflow jet or elsewhere behind the CL (Davis *et al., 2*004; Wheatly *et al., 2*006), along with the vortices. Rear inflow jets are orientated perpendicular to associated CLs, as distinct from the winds within the parallel-flowing (poleward) warm-conveyor belt, which is found ahead of many CLs in ETCs (Figure 1b; Browning 2004). Mesovortices and tornadoes produce the strongest gust in any direction, though more likely in the direction of the synoptic wind direction. Convective squall lines that present a strongly-bulging structure are referred to as bow echoes (Weisman 2001) and these systems can occur anywhere in Australia along fronts or trough lines (e.g. Keenan and Carbone 1992). Clark (2013) developed a climatology of CLs for the UK. To be classified as a CL, the feature has to meet threshold criteria (see table S1).

Extreme winds can also occur in the dry slot, through the dry conveyor belt (DCB) and convective systems within the dry slot (dry-slot convection; DSC). The DCB contains dry air descending from the upper troposphere or lower stratosphere, producing a region of clearing skies behind the cold front, which penetrates into the frontal cloud separating the

cloud head from the polar front cloud band. This forms the comma pattern seen in stage II-III (of the Shapiro-Keyser model) and as the cyclone develops further the cloud head wraps around the dry slot and begins to dissipate (Dacre *et al., 2*012). Strong winds are often experienced at the surface associated with the lower part of this sinking air (Cotton and Anthes, 1989), though Gray *et al.* (2011) state that the dry slot of an ETC is not usually associated with strong winds. Carr and Millard (1985) investigated the generation of a line of convection which formed in the centre of a dry intrusion during a Great Plains USA ETC event. They concluded that DSC can occur during the day through solar heating (in the cloud free dry slot) of the boundary layer, moist from the passing of the main area of convection. With surface moisture, warming, rising motion, adiabatic cooling and drying aloft a rapid destabilisation can occur, resulting in extreme convection and potentially vigorous rain and wind at the surface. Browning (2004) suggests that these are generated by differential rotation with height around the cyclone centre, creating overrunning of low-over-high wet-bulb potential air in the dry slot releasing potential instability.

Methods

The identification of each of the daily maximum gust speeds (DMGSs) to associated sub-synoptic-scale features (Figure 1b; described above in *Features*) is undertaken manually. The timing of each DMGS is available from the BoM to the nearest minute at each location and this is compared with the adjacent BoM surface pressure charts and ERA-Interim SLP data,

to show where each gust was in relation to the overall ETC. The satellite and radar images (which are available every 10 minutes, so no more than 5 minutes away from any given daily maximum gust) are then used to determine the specific feature (see Figure 1b) associated with each gust. When a DMGS is not judged to be associated with any sub-synoptic-scale feature, an assessment of the general pressure gradient over the site in question is conducted and the DMGS is subsequently identified as being caused by 'strong pressure gradient', if that is appropriate (i.e. isobars are tighter over the site than in other parts of the ETC), or remains unclassified. Once all of the DMGS have been categorised into sub-synoptic-scale features, they are then assembled, giving an insight of the main causes of the destructive winds. At many sites, there was no information on direction or timing of the gust, meaning that the feature could not be identified. Features that possess the same distinct characteristics to CLs, but do not reach the status of having a continuous line according to Clark (2013; see Table S1), are classified here as pseudoCLs.

This approach has never been utilised to analyse extreme winds associated with Australian ETCs. The method is similar to that used by Earl *et al.* (2017) for the UK, with the addition of the high spatial and temporal resolution geostationary Himawari satellite, making feature identification and tracking more accurate. The method is different from previous climatological studies of this type over Europe, for example Parton *et al.* (2010), Martínez-Alvarado *et al.* (2012) and Clark (2013), who used mid-tropospheric observations, radar

imagery and ERA-Interim data respectively, as these did not include observed windspeeds impacting the surface. It is also distinct from the approach of Hewson and Neu (2015) in their IMILAST project ('Intercomparison of MId-LAtitude STorm diagnostics', first described in Neu *et al., 2*013) analysis, based on storm track algorithms rather than surface based observations. We note that some extreme gusts may be missed by our method due to the spatially irregular nature of the observation network (Figure 4 – Part I), especially the smaller scale features such as tornadoes and mesovortices.

Results and discussion

Observed Features

One of the aims of this paper is to categorise the general features of the DMGSs. Figure 2 (and Table S2) highlights the features responsible during the ETC. The top 1% DMGSs (1DMGSs) on the 28th were dominated by the CL (and pseudoCL) and DSC, before the CCB came in later on in the day. The CCB was by far the biggest contributor on the 29th as the low-pressure-centre passed just south of Adelaide. Of the few top 5% DMGSs (5DMGSs) on the 30th, a small CC along the occluded front was the main contributor along with strong pressure gradient (PG) as the ETC moved eastward.

28th September

Our interpretation of the extreme DMGSs seen along the cold front on the 28th, reportedly responsible for the state-wide blackout, were caused by a distinctive CL, rather than individual supercells as reported (BoM, 2016). CLs, as described above (and in Table S1) and displayed in Figure 1, often produce tornadoes and mesovorticties, along with bow echoes and rear inflow jets.

Cellular convection

Ahead of the cold front (containing the CL), a convective cell formed on a trough (as marked by the BoM), affecting the Adelaide area about 4 hours prior to the cold front (see CC marked in Figure 3 Part I). This was not an organised line, hence termed as a convective cell. With the approaching CL not producing extreme DMGSs over Adelaide, this CC produced some of the strongest gusts of the day in the Adelaide Metropolitan area, however none were 1DMGSs as highlighted in Figure 6 – part I. The rain associated with this thundery CC, contributed to the severity of the CL on the cold front.

Convective line

Here, we analyse the CL, which could be split into sub categories (i.e. rear inflow jet, gust front, downburst etc.) however, for simplicity we categorise all DMGSs associated with the passing of this front with CL .We interpret the CL to have formed by 1500hrs ACST and no

longer was a coherent CL by 19:30hrs ACST based on Clark's (2013) criteria (despite being outside the 'cool season' (see Table S1)). This is based on the satellite (Figure 3 Part I) and radar images as mentioned in the method section. Before and after this period, the convection is still in a relatively organised line, rather than a rotational cell, so we refer to any associated DMGSs to be caused by a pseudoCL. CLs are overwhelmingly responsible for non-supercellular damaging winds from convective storms (Schenkman and Xue 2016) and this seems to be the case for this cold front. The damage associated with CLs tends not to be spatially uniform but rather marked over many small areas, as is the case here. The BoM (2016) report points to extremely strong low level wind shear, which is a crucial factor in the formation of bow echoes along CLs.

The top 0.1% DMGSs (0.1 DMGSs) which affected the surface stations, identified as being associated with the CL and pseudoCL, mainly had wind directions from the west to north-west (see Table S3), the direction of travel of the CL. This suggests that the winds were related to downdraughts beneath the heaviest rain bands or the rear inflow jet behind a bow in the CL, rather than northerlies which occurred ahead of the cold front. A rear inflow jet example is the 0.1DMGS experienced at Snowtown. The 3rd highest gust ever recorded here (since October 2003), the CL has a clear bow, as shown in Figure 3 marked by the black ovals. The gust occurred two minutes prior to the radar and satellite images and the site is directly behind the downburst causing the bow. Severe wind and hail (5cm in diameter)

were reported from this part of the CL with a tornado reported at Blyth (just southeast of Snowtown), 5 minutes after the radar and satellite images in Figure 3 where the heaviest rainfall is indicated, just south of the bow apex. This is typical of bow echoes as highlighted in the schematic in Figure 4, adapted for the southern hemisphere from Atkins *et al.* (2005). Yunta airstrip experienced its strongest ever gust, caused as the CL went through, directly beneath the very heavy precipitation, from the downburst as no tornado signals were reported at Yunta (BoM 2016).

Dry slot convection

As indicated by the green arrows in the infrared images in Figure 3 Part I, as the storm developed a mass of cloud formed behind (west) of the cold front and became wrapped up in the dry slot of the ETC. The cloud top temperature of this mass was not as low as the fronts, indicating that this is a region of moisture restricted to lower levels. This remained in the dry slot throughout the day, gradually turning to smaller cells (which reached higher levels with lower cloud top temperatures) by 01:30 ACST on the 29th (16:00 UTC) and disappeared during the night as the upper dry air descended and ceased from producing extreme gusts. It could be argued that this feature was part of the original cold front but became split. However, we feel that this region of moisture was not part of the main front or the main cloud head during development (see Figure 3 Part I).

This feature caused some extreme DMGSs over a large area in the west and centre of South Australia as shown in Figure 2. Figure 5 – part I shows that many of these were 0.1DMGSs. Tarcoola Aero, Nullarbor, Leigh Creek and Wudinna Aero all experienced top 6 ever gusts from DSC, highlighting the dangers of this feature, which remains relatively unstudied, compared to the conveyor belts and SJ. DSC affected Nullarbor (most westward site) at 13:39 ACST (03:49 UTC) as a large mass shown in Figure 3 Part I (green arrow – top right), the Adelaide area (Figure 5) at around 18:40 ACST (09:10 UTC) as a large cell, and Leigh Creek as separate small cell (which used to be part of a larger cell (Figure 5-top right panel red dot). This feature differs from the Carr and Millard (1985) example from the USA, where the generation of convection formed from a cloud-free dry slot due to solar radiation. Here, the low-level moisture was present throughout the dry slot formation, and changes from a low level large cloud mass to smaller cells throughout the day (28th) as shown in Figure 3 Part I. Browning (2004) suggests that DSC is generated by differential rotation with height around the cyclone centre, creating overrunning of low over high wet-bulb potential air in the dry slot releasing potential instability. There is evidence of this occurring here with higher cloud top temperature (darker grey), behind the main cold front (see Figure 3 Part I at 22:00 and 01:30 ACST) however, this was not the source of the damaging convection cells in this case. Figure 5 shows the lack of convectively available potential energy (CAPE) within the dry slot compared to the CL and bent back cloud, highlighting that the presence of deep moist convection was being subdued by the upper dry air. The sounding data from Adelaide airport (Figure 6) shows that the convection was limited to low- and mid-levels (500hPa)

within the dry slot (present at 21:30 ACST on the 28th). The cap is marked by the temperature inversion at 500hPa where the dry descending air met the low level moisture. This interaction is likely to have aided the strong downdraughts created by the evaporative cooling of this moisture. This raises the question of whether this is a rare example of 0.1DMGSs or whether this common extreme gust producing feature in the Great Australian Bight?

29th September

Cold conveyor belt

The CCB in ETC28 exhibited typical characteristics (see Browning 2004) occurring along the warm front towards the low-pressure-centre, where it spirals around the centre during stage IV of the Shapiro-Kayser model, marked as CCB in Figure 1b. This is indicated by the spiral cloud in Figure 3 Part I, with the CCB beneath the cloud signature. The CCB often descends to the surface (Clark *et al., 2*005; Baker, 2009), and here was associated with surface strong winds over a large area, part of which is shown by the scatterometer (Figure 7), highlighting the spatial extent and severity of the western part of the CCB as it flows around the low-pressure-centre. At this time (23:11 ACST; 13:41 UTC), the CCB began to effect the central coast, producing the strongest gusts of the 28th at four sites, including three 1DMGSs as highlighted in Figure 2. After midnight and into the 29th this was the dominant feature as the system moved eastwards. The low-pressure-centre tracked just

south of Adelaide and the CCB continued to wrap around the centre, multiple times, and caused a very high number of 1DMGSs and 0.1DMGSs throughout the day, with extreme winds caused throughout the spiralling CCB. Some were located towards the centre and some in the outer part of the spiral. The extremes at coastal sites Neptune Island and Ceduna (mention in part I) were due to the CCB, within the outer spiral of the cloud signature, to the east of the low-pressure-centre (Figure 3 Part I at 16:00 and 21:00 UTC). The gust seen at Whyalla Aero was the only DMGSs which occurred outside of the cloud signature and with no visible convective cell in the vicinity, so was considered to be part of a jet reaching the surface from within the dry intrusion (not associated with DSC) which was spiralling (with the CCB) around the low-pressure-centre. This part of the dry slot is apparent in the 9:30 ACST sounding from Adelaide airport on the 29th (Figure 6), above the low-level CCB jet which was producing very strong near-surface winds of 50 Knots. The 21:30 ACST sounding on the 29th is located within the main CCB and is close to saturation from the lower to upper troposphere. The DMGSs seen on the 29th, especially on the central coast sites, were more extreme than on the 28th all associated with the CCB spiralling around the low-pressure-centre. Most gusts were from a westerly direction, combining the CCB with the ETC28's eastward translation.

30th September

A convective cell formed along the occluded front which was the cause of many 5DMGSs west of the low-pressure-centre. Strong PG also was the cause of DMGSs on the 30th, bringing strong south-westerlies to eastern South Australia.

Overall impact

Table 1 summarises the subjectively classified features associated with all DMGSs during ETC28. The CCB was by far the biggest contributor to the 5% and 1DMGSs accounting for half of the former and 60% of the latter. These conveyor belts are widely known to regularly cause extreme surface winds within European ETCs (e.g. Browning 2004; Hewson and Neu 2015; Earl *et al., 2*017), and our analysis shows that this is the case for ETC28 within Australia. This is not surprising as this feature covers a wide swath as the ETC tracks east, though as we show here it also produces extreme surface winds, contributing to almost half of the 0.1DMGSs. DSC was a major factor in ETC28 accounting for almost a quarter of the 17 0.1DMGSs seen during ETC28. Earl *et al.* (2017) found no cases of DSC contributing to 0.1DMGSs over a 7-year climatology in the UK so, as mentioned, it is unclear as to whether the moisture intruding into the dry slot in this manner is a common occurrence in the Bight, and this warrants further analysis. The CL/ pseudoCL was a very important feature of ETC28 and was responsible for the widely reported South Australia blackout. In this analysis however, we find that it wasn't the dominant cause of the strongest gusts. A major characteristic this feature is that gusts associated with CLs are not continuous and enhanced

over many small sections, so some gusts are likely to have been missed by the observation network.

Conclusions

The ETC that brought South Australia to a standstill on the 28th-30th September 2016, contained many characteristics and mesoscale features to those observed in ETCs over western Europe. ETC28 deepened more explosively than all but two over the past 37 years and contained the lowest central pressure as explored in part I of this paper. The widely studied cold-conveyer belt was by far the biggest contributor to extreme gusts; however, convective systems within the dry slot caused a large amount of extremes. The extreme gust causing DSC rarely causes extreme gusts in ETCs over the UK, so warrants further analysis to examine whether this is common extreme gust-producing ETC feature over southern Australian and the Great Australian Bight ETCs. The convective line along the main cold front was a very violent feature of ETC28 and was responsible for the widely reported South Australia blackout.

Acknowledgements

Parts of this research were made possible by funding from the Australian Research Council (ARC) Grant DP16010997. Nick Earl was also supported by the ARC (CE110001028).

References

Atkins NT, Bouchard CS, Przybylinski RW, Trapp RJ, Schmocker G. 2005. Damaging surface wind mechanisms within the 10 June 2003 Saint Louis bow echo during BAMEX. *Mon. Weather. Rev.*, 133(8): 2275-2296

Baker L. 2009. Sting jets in severe northern European wind storms. *Weather.* 64(6): 143-148.

Browning KA. 2004. The sting at the end of the tail: Damaging winds associated with extratropical cyclones. *Q. J. R. Meteorol. Soc.* 130: 375-399. doi: 10.1256/qj.02.143.

Bureau of Meteorology. 2016. Severe thunderstorm and tornado outbreak South Australia 28 September 2016. 54 pp. http://www.bom.gov.au/announcements/sevwx/sa/Severe_Thunderstorm_and_Tornado_Outbreak_28_September_2016.pdf.

Carlson TN. 1980. Airflow Through Midlatitude Cyclones and the Comma Cloud Pattern. *Mon. Weather. Rev.* 108: 1498–1509.

Carr FH, Millard JP. 1985. A composite study of comma clouds and their association with severe weather over the Great Plains. *Mon. Weather. Rev.* 113: 370–387.

Clark PA, Browning KA, Wang C. 2005. The sting at the end of the tail: Model diagnostics of fine-scale three-dimensional structure of the cloud head. *Q. J. R. Meteorol. Soc.* 131(610): 2263-2292.

Clark MR. 2013. A Provisional Climatology of Cool-Season Convective Lines in the UK. *Atmos. Res.* 123: 180-196.

Cotton WR, Anthes R. 1989. *Storm and Cloud Dynamics.* Academic Press; 883 pp.

Dacre HF, Hawcroft MK, Stringer MA, Hodges KI. 2012. An Extratropical Cyclone Atlas: A Tool for Illustrating Cyclone Structure and Evolution Characteristics. *Bull. Am. Meteorol. Soc.* 93(10): 1497-1502.

Davis C, Atkins N, Bartels D, Bosart L, Coniglio M, Bryan G, Cotton W, Dowell D, Jewett B, Johns R, Jorgensen D. 2004. The bow echo and MCV experiment: Observations and opportunities. *Bull. Am. Meteorol. Soc.* 85: 1075–1093.

Earl N, Dorling S, Starks M, Finch R. 2017. Subsynoptic-scale features associated with extreme surface gusts in UK extratropical cyclone events. *Geophys. Res. Lett.* 44: 3932–3940. doi:10.1002/2017GL073124.

Fink AH, Brücher T, Ermert V, Krüger A, Pinto JG. 2009. The European storm Kyrill in January 2007: synoptic evolution, meteorological impacts and some considerations with respect to climate change. *Natural Hazards and Earth System Sciences*, 9(2): 405-423.

Gray SL, Martínez-Alvarado O, Baker LH, Clark PA. 2011. Conditional symmetric instability in sting-jet storms. *Q. J. R. Meteorol. Soc.* 137(659): 1482-1500.

Hewson TD, Neu U. 2015. Cyclones, windstorms and the IMILAST project, *Tellus A*, 67: 27128.

Keenan TD, Carbone RE. 1992. A preliminary morphology of precipitation systems in tropical northern Australia. *Q. J. R. Meteorol. Soc.* 118(504): 283-326.

Martínez-Alvarado O, Gray SL, Catto JL, Clark PA. 2012. Sting jets in intense winter North-Atlantic windstorms. *Environ. Res. Lett.* 7: 024014.

Neu U, Akperov MG, Bellenbaum N, Benestad R, Blender R, Caballero R, Cocozza A, Dacre HF, Feng Y, Fraedrich K, Grieger J. 2013. IMILAST: A community effort to intercompare extratropical cyclone detection and tracking algorithms. *Bull. Am. Meteorol. Soc.* 94: 529-547. doi: 10.1175/BAMS-D-11-00154.1

Parton G, Dore A, Vaughan G. 2010. A climatology of midtropospheric mesoscale strong wind events as observed by the MST radar, Aberystwyth. *Meteorol. Appl.* 17: 340–354. doi:10.1002/met.203.

Schenkman AD, Xue M. 2016. Bow-echo mesovortices: A review. *Atmos. Res.* 170: 1-13. doi: 10.1016/j.atmosres.2015.11.003

Schultz DM. 2001. Reexamining the cold conveyor belt. *Mon. Weather. Rev.* 129: 2205-2225.

Schultz DM, Browning KA. 2017. What is a sting jet? *Weather.* 72(3): 63-66.

Shapiro MA, Keyser DA. 1990. Fronts, jet streams, and the tropopause. *Extratropical Cyclones: The Erik Palmén Memorial Volume*, C. W. Newton and E. O. Holopainen, Eds. *Am. Meteorol. Soc.* 167–191.

Slater TP, Schultz DM, Vaughan G. 2015. Acceleration of near-surface strong winds in a dry, idealized extratropical cyclone. *Q. J. R. Meteorol. Soc.* 141: 1004–1016. doi:10.1002/qj.2417

Smart DJ, Browning KA. 2014. Attribution of strong winds to a cold conveyor belt and sting jet. *Q. J. R. Meteorol. Soc.* 140: 595–610

Weisman ML. 2001. Bow echoes: A tribute to TT Fujita. *Bull. Am. Meteorol. Soc.* 82(1): 97-116.

Wheatley DM, Trapp RJ, Atkins NT. 2006. Radar and damage analysis of severe bow echoes observed during BAMEX. *Mon. Weather Rev.* 134(3): 791-806.

Feature	5%	1%	0.1%
CCB	46	33	8
CC	12	1	0
DSC	11	6	4
CL	8	5	3
Pseudo-CL	7	7	2
DCB	3	3	0
Strong PG	3	0	0
WCB	1	0	0

Table 1 – Total number of DMGSs of all the contributing features during the passage of ETC28 for the three thresholds.

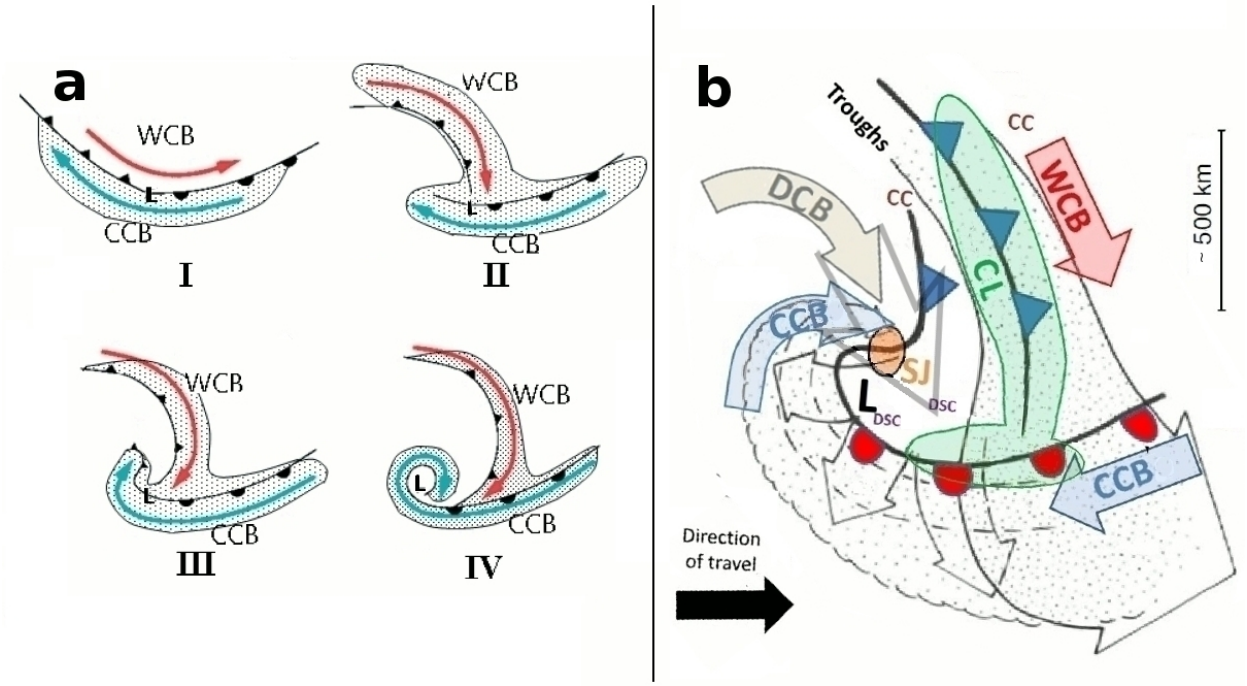

Figure 1. a. Shapiro-Keyser conceptual model of the life cycle of an extra-tropical cyclone: (I) open wave, (II) frontal fracture, (III) bent-back front and frontal T-bone, and (IV) mature, frontal seclusion (adapted for the southern hemisphere). The cold and warm conveyor belts (CCB and WCB respectively) are marked along with the low pressure centre (L) and the cloud signature (stippled areas) (adapted from Baker, 2009). b. Conceptual model of sub-synoptic-scale features within an extra-tropical cyclone, during transition from stage III to stage IV (adapted from Browning, 2004, for the southern hemisphere). Also displays where convective system (CC), dry slot convection (DSC), dry conveyor belt (DCB), convective line (CL) and sting jet (SJ) associated gusts can occur in relation to the cyclone.

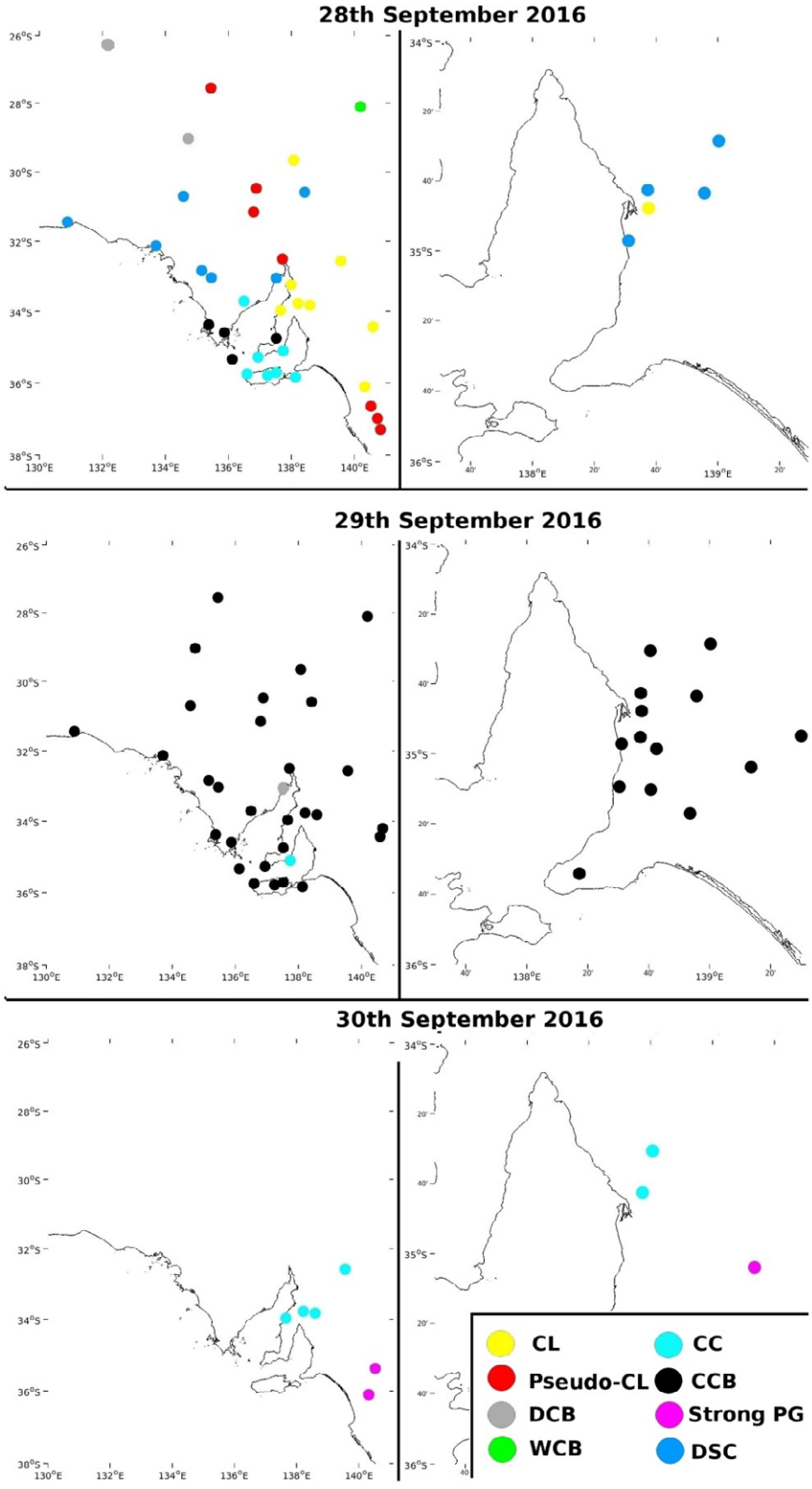

Figure 2. Location of gust and associated feature for the top 5% of DMGSs affecting the surface on the 28th, 29th and 30th September 2016. The whole of South Australia is displayed on the left panels and the Adelaide area on the right panels for clarity.

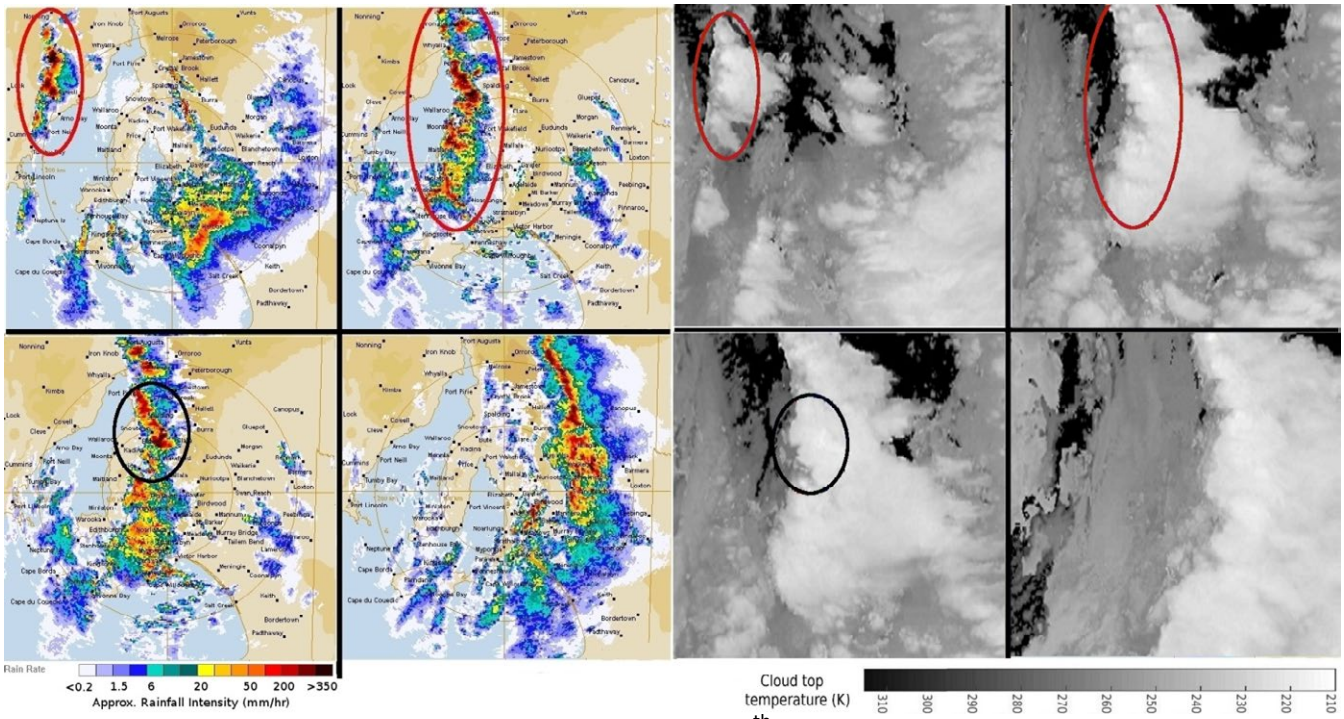

Figure 3 – Radar and satellite infrared images from the 28th September 2016 at 13:20 ACST (top left) 15:00ACST (top right), 15:20ACST (bottom left) and 17:20ACST (bottom right). The red ovals show the CL development and black highlight the bow shape causing the intense gust at Snowtown.

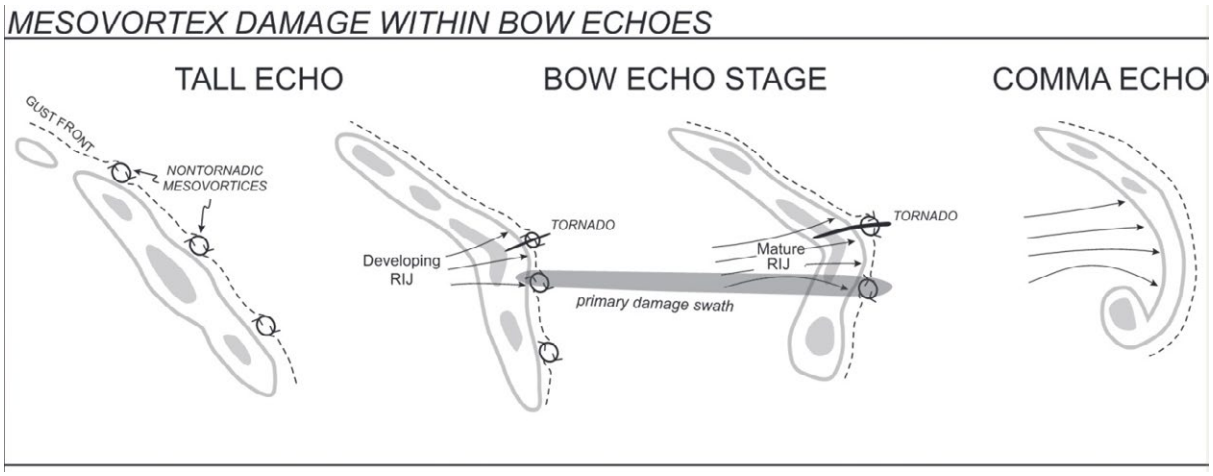

Figure 4 – Schematic diagram of a bow echo and attendant damage produced by mesovortices adapted (from Atkins *et al.*, 2005) for the southern hemisphere.

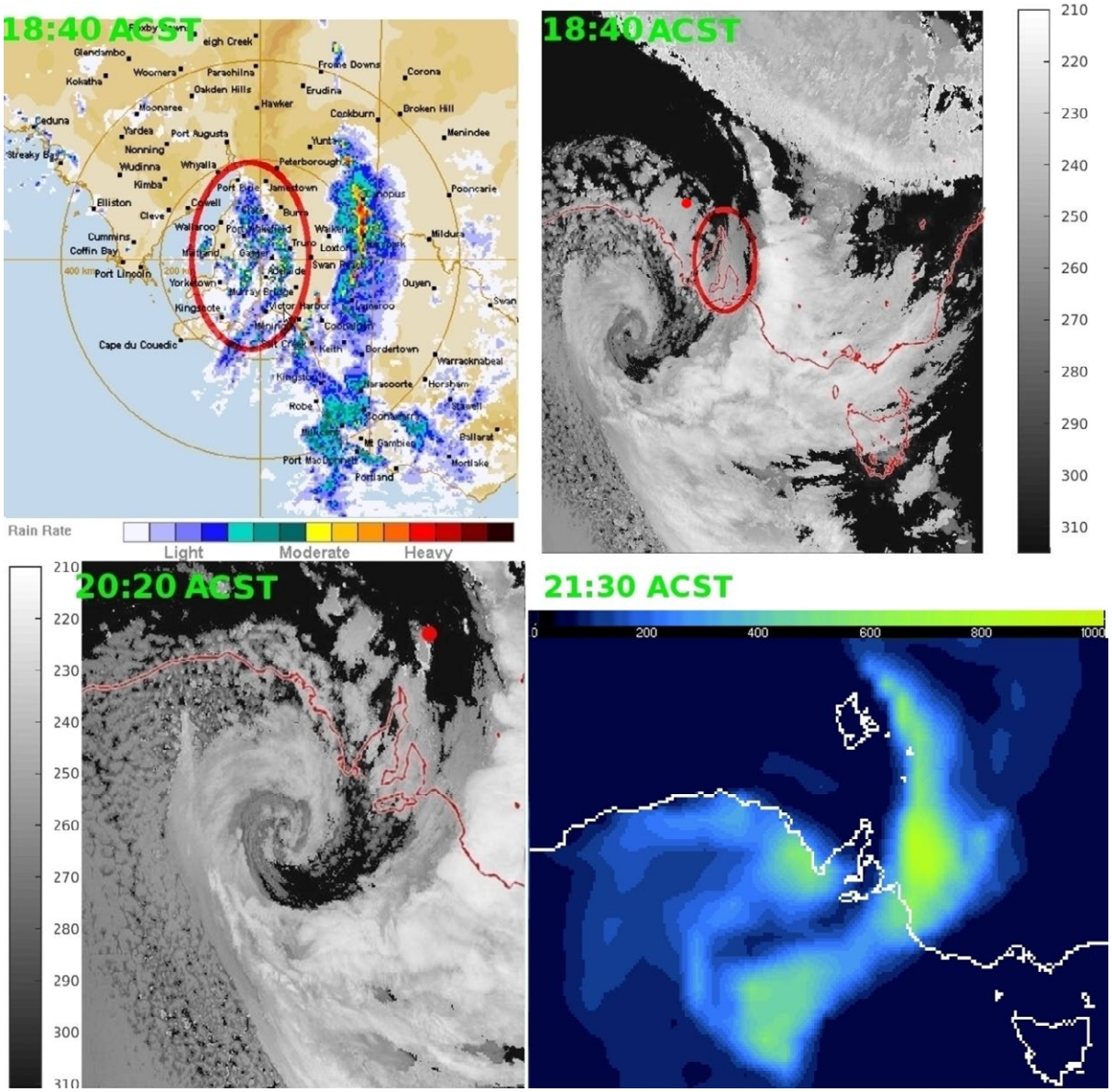

Figure 5 – Radar (rainfall rate) and infrared (cloud to temperature in Kelvin) highlighting DSC over the Adelaide Metrapolitan area at 18:40 ACST on the 28th September 2016 and infrared image displaying the cell at Leigh Creek (red dot) at 20:20 ACST (DMGS at Leigh Creek occurred at 20:19 ACST). The red dot in the 18:40 ACST infrared image displays the location of the DSC which later affected Leigh Creek. Also displayed is the convectively available potential energy (CAPE) from ERA-interim (J kg^{-1}) 12 hour forecast for 21:30 ACST.

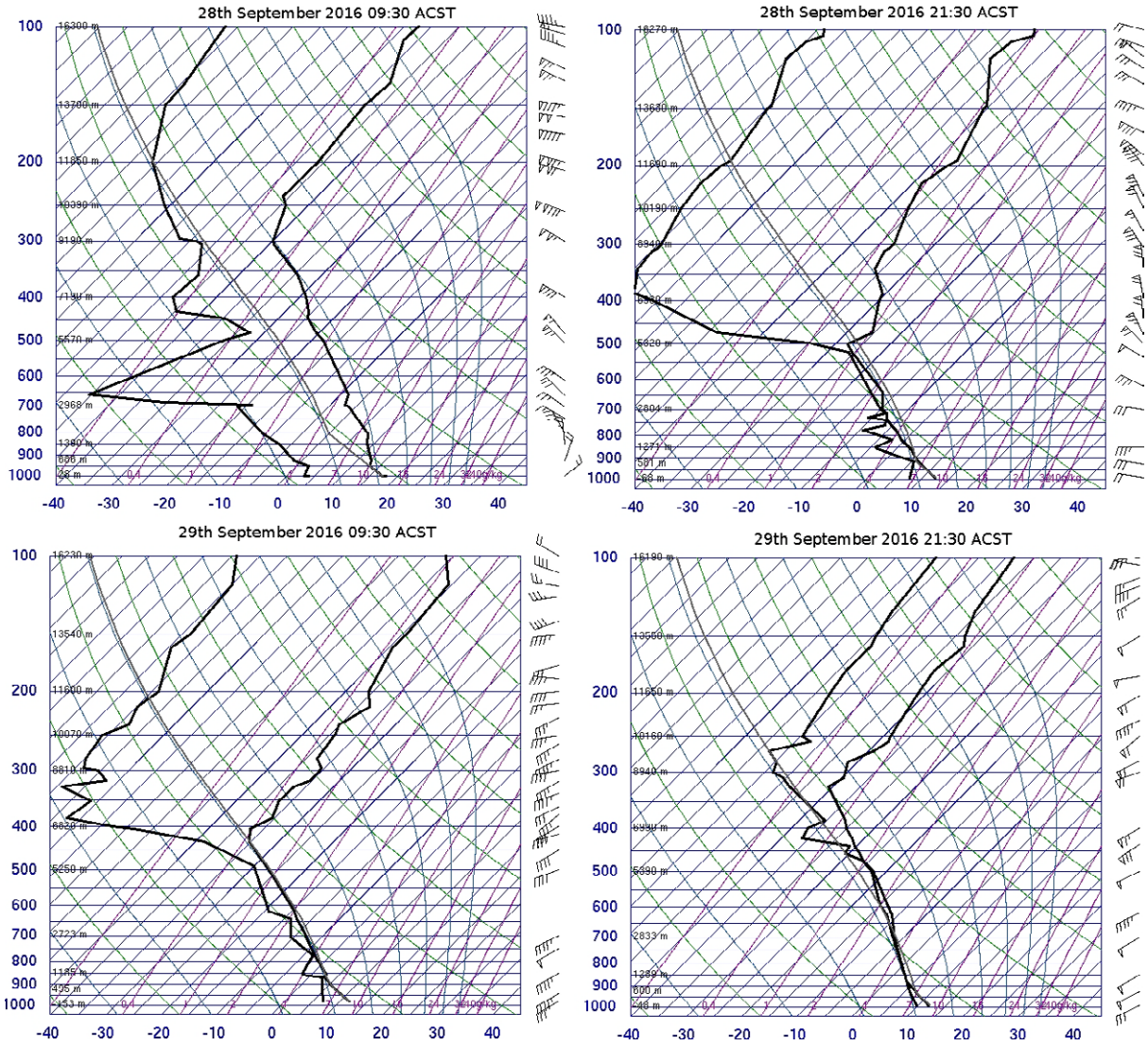

Figure 6 – Atmospheric soundings from Adelaide Airport on the 28th and 29th September 2016 from the University of Wyoming (available from http://weather.uwyo.edu/upperair/sounding.html). Right hand lines represent temperature and left dew point temperature in degrees Celsius. Wind barbs follow standard notation (small barb - 5 Knots, long barb – 10 Knots, triangle – 50 Knots and directions from where the wind is coming).

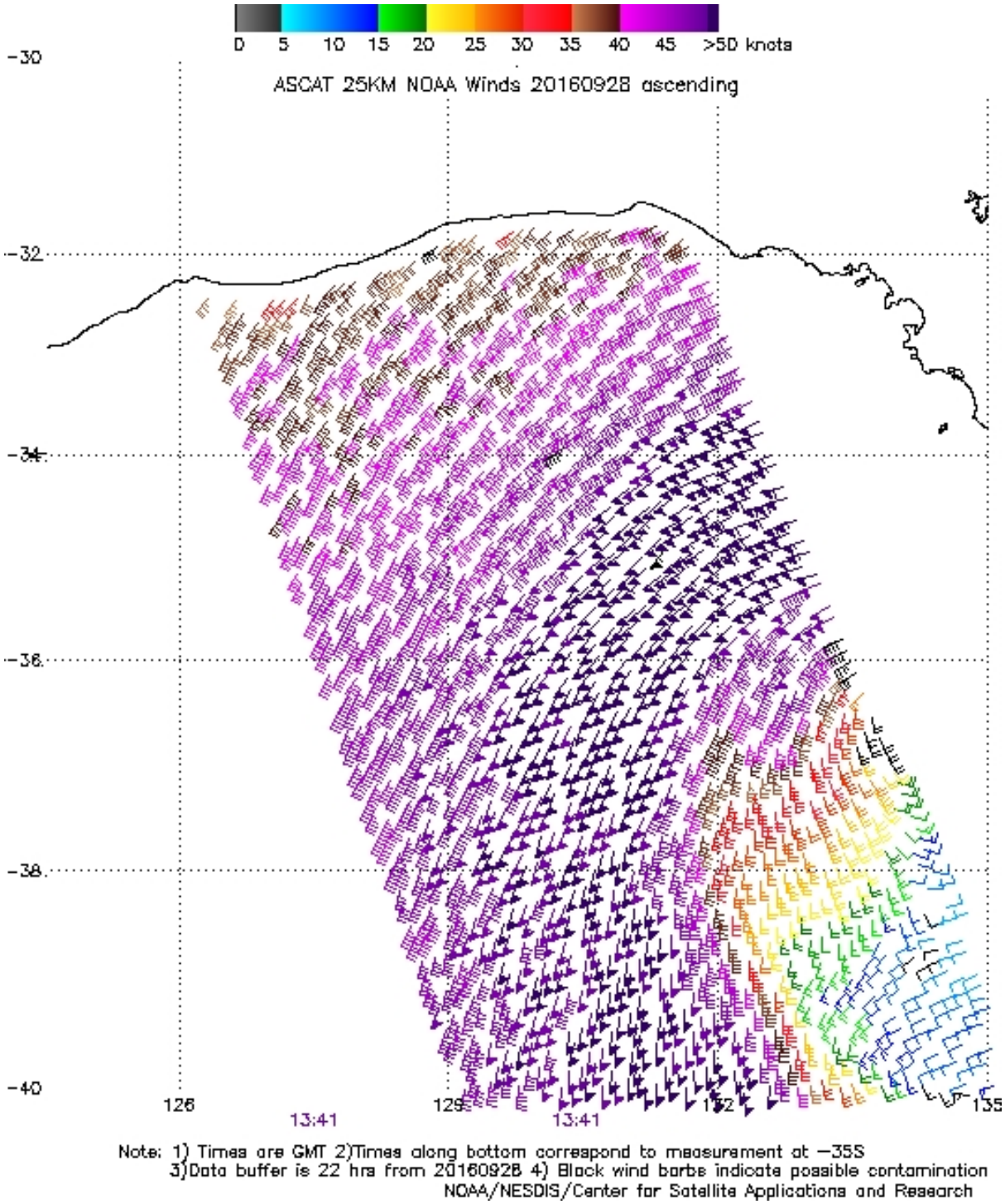

Figure 7 – ASCAT scatterometer (from https://manati.star.nesdis.noaa.gov/datasets/ASCATData.php) highlighting the extent of the CCB winds over the Bight at 23:11 ACST (13:41 UTC) on the 28th September

Sub-synoptic-scale features associated with extreme surface gusts during the South Australia Storm of September 2016 – Part II: Analysis of mechanisms driving the gusts

Nick Earl*[1,2] and Ian Simmonds[1]

[1] School of Earth Sciences, The University of Melbourne, Parkville, Melbourne, Victoria, 3010, Australia.

[2] Institute for Marine and Antarctic Studies, The University of Tasmania, Hobart, Tasmania, 7003, Australia.

*corresponding author – nearl@unimelb.edu.au

Abstract

An extreme extra-tropical cyclone (ETC) struck South Australia on the 28th September 2016, causing state-wide blackouts and damage. In the second part of this two part study, we examine the extreme surface wind producing mechanisms within the ETC. ETCs have been extensively studied in the northern hemisphere (particularly in western Europe), highlighting the gust-producing mesoscale features within. Before now, no southern hemisphere ETC has been examined in this way. There were a number of extreme gust-producing features within the ETC, comparable to those observed in storms over western Europe. These included a convective line, which caused many of the most extreme gusts and knocked out the state power grid. However, dry slot convection also contributed to the extremes and this feature is known to rarely cause extreme gusts in ETCs over the UK, so warrants further analysis to examine whether this is common extreme gust-producing ETC feature over southern Australia. The strongest winds recorded throughout the event occurred on the 29th September, and these were associated with the cold conveyor belt which spiralled around the low-pressure-centre.

Introduction

On the 28th September 2016, an extreme ETC (Extra-tropical cyclone; hereafter ETC28) affected the Australian state of South Australia causing state-wide blackouts and damage. In part 1 of this paper we determined that ETC28 progressed along a common track and followed the Shapiro-Keyser life cycle model often seen in explosive European ETCs. We constructed a track analysis of the event and of similar-tracking ETCs and found that ETC28's low pressure centre deepened more explosively than all but two other ETCs over the past 37 years and reached the lowest central pressure of all. We found that ETC28 potentially contained a sting jet (SJ; Browning 2004); however, if made it to the surface, it was not the cause of the state-wide damage. The ETC centre did not reach landfall until well into stage IV of its life cycle around 0000 UTC on the 29th (Figure 1a) and SJs occur during stages II-III. Here, we focus on the mesoscale features within ETC28 that did cause the most severe surface wind gusts. We also establish whether this Australian ETC exhibited similar features to those seen over western Europe. This is the first southern hemisphere ETC to be split into different sub-synoptic scale features in this way, with its extremity based on surface wind observations.

Features

Within ETCs, there are many mesoscale features which can produce extreme surface winds, and a full description of these features is presented by Earl *et al.* (2017) and in Table S1. Some occur only within explosively deepening ETCs, while others occur in any ETC or (less often) independently. Having established that the extreme winds seen during ETC28 were not associated with a SJ, we explore the other features, which were responsible. Baker

(2009) found that extreme surface winds during a UK ETC, Gudrun of January 2005, were associated with the cold conveyor belt (CCB; see Carlson, 1980; Schultz 2001) as it spiralled around the low-pressure-centre on the bent back front and acted in the same direction as the motion of the cyclone (Figure 1b). This was also the case over Germany during windstorm Kyrill in 2007, where there was no SJ identified but intense surface winds occurred in this part of the ETC (Fink et al., 2009). This shows that the CCB can cause high-impact gusts without the presence of a SJ and indeed be the dominant cause of extreme gusts, as Earl *et al.* (2017) concluded using a climatology of UK ETCs. Evidence for both the CCB and SJ causing strong surface winds was presented during the development of UK ETC Ulli (January 2012) by Smart and Browning (2014), and in the broader general discussion of Schultz and Browning (2017). Slater *et al.* (2015) supported this by conducting an idealised study, using the high-resolution Weather Research and Forecasting model to investigate the fine structure of the cloud head and found that separate discrete surface gust maxima during the early stage of frontal fracture.

Earl *et al.* (2017) found convective lines (CLs), comprised of narrow cold frontal rain-bands and post-frontal quasi-linear convective systems, accounted for a third of the strongest 1980-2014 surface gusts observed in the UK. CLs (Figure 1b) are well-known for producing strong winds, including intense downburst winds, a rear inflow jet (Weisman 2001), low-level mesovortices and tornadoes. These systems may produce highly damaging straight-line (non-rotational) winds as part of the rear inflow jet or elsewhere behind the CL (Davis *et al., 2*004; Wheatly *et al., 2*006), along with the vortices. Rear inflow jets are orientated perpendicular to associated CLs, as distinct from the winds within the parallel-flowing (poleward) warm-conveyor belt, which is found ahead of many CLs in ETCs (Figure 1b;

Browning 2004). Mesovortices and tornadoes produce the strongest gust in any direction, though more likely in the direction of the synoptic wind direction. Convective squall lines that present a strongly-bulging structure are referred to as bow echoes (Weisman 2001) and these systems can occur anywhere in Australia along fronts or trough lines (e.g. Keenan and Carbone 1992). Clark (2013) developed a climatology of CLs for the UK. To be classified as a CL, the feature has to meet threshold criteria (see table S1).

Extreme winds can also occur in the dry slot, through the dry conveyor belt (DCB) and convective systems within the dry slot (dry-slot convection; DSC). The DCB contains dry air descending from the upper troposphere or lower stratosphere, producing a region of clearing skies behind the cold front, which penetrates into the frontal cloud separating the cloud head from the polar front cloud band. This forms the comma pattern seen in stage II-III (of the Shapiro-Keyser model) and as the cyclone develops further the cloud head wraps around the dry slot and begins to dissipate (Dacre *et al., 2*012). Strong winds are often experienced at the surface associated with the lower part of this sinking air (Cotton and Anthes, 1989), though Gray *et al.* (2011) state that the dry slot of an ETC is not usually associated with strong winds. Carr and Millard (1985) investigated the generation of a line of convection which formed in the centre of a dry intrusion during a Great Plains USA ETC event. They concluded that DSC can occur during the day through solar heating (in the cloud free dry slot) of the boundary layer, moist from the passing of the main area of convection. With surface moisture, warming, rising motion, adiabatic cooling and drying aloft a rapid destabilisation can occur, resulting in extreme convection and potentially vigorous rain and wind at the surface. Browning (2004) suggests that these are generated by differential

rotation with height around the cyclone centre, creating overrunning of low-over-high wet-bulb potential air in the dry slot releasing potential instability.

Methods

The identification of each of the daily maximum gust speeds (DMGSs) to associated sub-synoptic-scale features (Figure 1b; described above in *Features*) is undertaken manually. The timing of each DMGS is available from the BoM to the nearest minute at each location and this is compared with the adjacent BoM surface pressure charts and ERA-Interim SLP data, to show where each gust was in relation to the overall ETC. The satellite and radar images (which are available every 10 minutes, so no more than 5 minutes away from any given daily maximum gust) are then used to determine the specific feature (see Figure 1b) associated with each gust. When a DMGS is not judged to be associated with any sub-synoptic-scale feature, an assessment of the general pressure gradient over the site in question is conducted and the DMGS is subsequently identified as being caused by 'strong pressure gradient', if that is appropriate (i.e. isobars are tighter over the site than in other parts of the ETC), or remains unclassified. Once all of the DMGS have been categorised into sub-synoptic-scale features, they are then assembled, giving an insight of the main causes of the destructive winds. At many sites, there was no information on direction or timing of the gust, meaning that the feature could not be identified. Features that possess the same distinct characteristics to CLs, but do not reach the status of having a continuous line according to Clark (2013; see Table S1), are classified here as pseudoCLs.

This approach has never been utilised to analyse extreme winds associated with Australian ETCs. The method is similar to that used by Earl *et al.* (2017) for the UK, with the addition of the high spatial and temporal resolution geostationary Himawari satellite, making feature identification and tracking more accurate. The method is different from previous climatological studies of this type over Europe, for example Parton *et al.* (2010), Martínez-Alvarado *et al.* (2012) and Clark (2013), who used mid-tropospheric observations, radar imagery and ERA-Interim data respectively, as these did not include observed windspeeds impacting the surface. It is also distinct from the approach of Hewson and Neu (2015) in their IMILAST project ('Intercomparison of MId-LAtitude STorm diagnostics', first described in Neu *et al., 2*013) analysis, based on storm track algorithms rather than surface based observations. We note that some extreme gusts may be missed by our method due to the spatially irregular nature of the observation network (Figure 4 – Part I), especially the smaller scale features such as tornadoes and mesovortices.

Results and discussion

Observed Features

One of the aims of this paper is to categorise the general features of the DMGSs. Figure 2 (and Table S2) highlights the features responsible during the ETC. The top 1% DMGSs (1DMGSs) on the 28th were dominated by the CL (and pseudoCL) and DSC, before the CCB came in later on in the day. The CCB was by far the biggest contributor on the 29th as the low-pressure-centre passed just south of Adelaide. Of the few top 5% DMGSs (5DMGSs) on

the 30th, a small CC along the occluded front was the main contributor along with strong pressure gradient (PG) as the ETC moved eastward.

28th September

Our interpretation of the extreme DMGSs seen along the cold front on the 28th, reportedly responsible for the state-wide blackout, were caused by a distinctive CL, rather than individual supercells as reported (BoM, 2016). CLs, as described above (and in Table S1) and displayed in Figure 1, often produce tornadoes and mesovorticties, along with bow echoes and rear inflow jets.

Cellular convection

Ahead of the cold front (containing the CL), a convective cell formed on a trough (as marked by the BoM), affecting the Adelaide area about 4 hours prior to the cold front (see CC marked in Figure 3 Part I). This was not an organised line, hence termed as a convective cell. With the approaching CL not producing extreme DMGSs over Adelaide, this CC produced some of the strongest gusts of the day in the Adelaide Metropolitan area, however none were 1DMGSs as highlighted in Figure 6 – part I. The rain associated with this thundery CC, contributed to the severity of the CL on the cold front.

Convective line

Here, we analyse the CL, which could be split into sub categories (i.e. rear inflow jet, gust front, downburst etc.) however, for simplicity we categorise all DMGSs associated with the passing of this front with CL .We interpret the CL to have formed by 1500hrs ACST and no longer was a coherent CL by 19:30hrs ACST based on Clark's (2013) criteria (despite being outside the 'cool season' (see Table S1)). This is based on the satellite (Figure 3 Part I) and radar images as mentioned in the method section. Before and after this period, the convection is still in a relatively organised line, rather than a rotational cell, so we refer to any associated DMGSs to be caused by a pseudoCL. CLs are overwhelmingly responsible for non-supercellular damaging winds from convective storms (Schenkman and Xue 2016) and this seems to be the case for this cold front. The damage associated with CLs tends not to be spatially uniform but rather marked over many small areas, as is the case here. The BoM (2016) report points to extremely strong low level wind shear, which is a crucial factor in the formation of bow echoes along CLs.

The top 0.1% DMGSs (0.1 DMGSs) which affected the surface stations, identified as being associated with the CL and pseudoCL, mainly had wind directions from the west to north-west (see Table S3), the direction of travel of the CL. This suggests that the winds were related to downdraughts beneath the heaviest rain bands or the rear inflow jet behind a bow in the CL, rather than northerlies which occurred ahead of the cold front. A rear inflow jet example is the 0.1DMGS experienced at Snowtown. The 3rd highest gust ever recorded here (since October 2003), the CL has a clear bow, as shown in Figure 3 marked by the black ovals. The gust occurred two minutes prior to the radar and satellite images and the site is directly behind the downburst causing the bow. Severe wind and hail (5cm in diameter)

were reported from this part of the CL with a tornado reported at Blyth (just southeast of Snowtown), 5 minutes after the radar and satellite images in Figure 3 where the heaviest rainfall is indicated, just south of the bow apex. This is typical of bow echoes as highlighted in the schematic in Figure 4, adapted for the southern hemisphere from Atkins *et al.* (2005). Yunta airstrip experienced its strongest ever gust, caused as the CL went through, directly beneath the very heavy precipitation, from the downburst as no tornado signals were reported at Yunta (BoM 2016).

Dry slot convection

As indicated by the green arrows in the infrared images in Figure 3 Part I, as the storm developed a mass of cloud formed behind (west) of the cold front and became wrapped up in the dry slot of the ETC. The cloud top temperature of this mass was not as low as the fronts, indicating that this is a region of moisture restricted to lower levels. This remained in the dry slot throughout the day, gradually turning to smaller cells (which reached higher levels with lower cloud top temperatures) by 01:30 ACST on the 29th (16:00 UTC) and disappeared during the night as the upper dry air descended and ceased from producing extreme gusts. It could be argued that this feature was part of the original cold front but became split. However, we feel that this region of moisture was not part of the main front or the main cloud head during development (see Figure 3 Part I).

This feature caused some extreme DMGSs over a large area in the west and centre of South Australia as shown in Figure 2. Figure 5 – part I shows that many of these were 0.1DMGSs.

Tarcoola Aero, Nullarbor, Leigh Creek and Wudinna Aero all experienced top 6 ever gusts from DSC, highlighting the dangers of this feature, which remains relatively unstudied, compared to the conveyor belts and SJ. DSC affected Nullarbor (most westward site) at 13:39 ACST (03:49 UTC) as a large mass shown in Figure 3 Part I (green arrow – top right), the Adelaide area (Figure 5) at around 18:40 ACST (09:10 UTC) as a large cell, and Leigh Creek as separate small cell (which used to be part of a larger cell (Figure 5-top right panel red dot). This feature differs from the Carr and Millard (1985) example from the USA, where the generation of convection formed from a cloud-free dry slot due to solar radiation. Here, the low-level moisture was present throughout the dry slot formation, and changes from a low level large cloud mass to smaller cells throughout the day (28th) as shown in Figure 3 Part I. Browning (2004) suggests that DSC is generated by differential rotation with height around the cyclone centre, creating overrunning of low over high wet-bulb potential air in the dry slot releasing potential instability. There is evidence of this occurring here with higher cloud top temperature (darker grey), behind the main cold front (see Figure 3 Part I at 22:00 and 01:30 ACST) however, this was not the source of the damaging convection cells in this case. Figure 5 shows the lack of convectively available potential energy (CAPE) within the dry slot compared to the CL and bent back cloud, highlighting that the presence of deep moist convection was being subdued by the upper dry air. The sounding data from Adelaide airport (Figure 6) shows that the convection was limited to low- and mid-levels (500hPa) within the dry slot (present at 21:30 ACST on the 28th). The cap is marked by the temperature inversion at 500hPa where the dry descending air met the low level moisture. This interaction is likely to have aided the strong downdraughts created by the evaporative cooling of this moisture. This raises the question of whether this is a rare example of

0.1DMGSs or whether this common extreme gust producing feature in the Great Australian Bight?

29th September

Cold conveyor belt

The CCB in ETC28 exhibited typical characteristics (see Browning 2004) occurring along the warm front towards the low-pressure-centre, where it spirals around the centre during stage IV of the Shapiro-Kayser model, marked as CCB in Figure 1b. This is indicated by the spiral cloud in Figure 3 Part I, with the CCB beneath the cloud signature. The CCB often descends to the surface (Clark *et al., 2*005; Baker, 2009), and here was associated with surface strong winds over a large area, part of which is shown by the scatterometer (Figure 7), highlighting the spatial extent and severity of the western part of the CCB as it flows around the low-pressure-centre. At this time (23:11 ACST; 13:41 UTC), the CCB began to effect the central coast, producing the strongest gusts of the 28th at four sites, including three 1DMGSs as highlighted in Figure 2. After midnight and into the 29th this was the dominant feature as the system moved eastwards. The low-pressure-centre tracked just south of Adelaide and the CCB continued to wrap around the centre, multiple times, and caused a very high number of 1DMGSs and 0.1DMGSs throughout the day, with extreme winds caused throughout the spiralling CCB. Some were located towards the centre and some in the outer part of the spiral. The extremes at coastal sites Neptune Island and Ceduna (mention in part I) were due to the CCB, within the outer spiral of the cloud signature, to the east of the low-pressure-centre (Figure 3 Part I at 16:00 and 21:00 UTC).

The gust seen at Whyalla Aero was the only DMGSs which occurred outside of the cloud signature and with no visible convective cell in the vicinity, so was considered to be part of a jet reaching the surface from within the dry intrusion (not associated with DSC) which was spiralling (with the CCB) around the low-pressure-centre. This part of the dry slot is apparent in the 9:30 ACST sounding from Adelaide airport on the 29th (Figure 6), above the low-level CCB jet which was producing very strong near-surface winds of 50 Knots. The 21:30 ACST sounding on the 29th is located within the main CCB and is close to saturation from the lower to upper troposphere. The DMGSs seen on the 29th, especially on the central coast sites, were more extreme than on the 28th all associated with the CCB spiralling around the low-pressure-centre. Most gusts were from a westerly direction, combining the CCB with the ETC28's eastward translation.

30th September

A convective cell formed along the occluded front which was the cause of many 5DMGSs west of the low-pressure-centre. Strong PG also was the cause of DMGSs on the 30th, bringing strong south-westerlies to eastern South Australia.

Overall impact

Table 1 summarises the subjectively classified features associated with all DMGSs during ETC28. The CCB was by far the biggest contributor to the 5% and 1DMGSs accounting for half of the former and 60% of the latter. These conveyor belts are widely known to regularly cause extreme surface winds within European ETCs (e.g. Browning 2004; Hewson and Neu

2015; Earl *et al., 2*017), and our analysis shows that this is the case for ETC28 within Australia. This is not surprising as this feature covers a wide swath as the ETC tracks east, though as we show here it also produces extreme surface winds, contributing to almost half of the 0.1DMGSs. DSC was a major factor in ETC28 accounting for almost a quarter of the 17 0.1DMGSs seen during ETC28. Earl *et al.* (2017) found no cases of DSC contributing to 0.1DMGSs over a 7-year climatology in the UK so, as mentioned, it is unclear as to whether the moisture intruding into the dry slot in this manner is a common occurrence in the Bight, and this warrants further analysis. The CL/ pseudoCL was a very important feature of ETC28 and was responsible for the widely reported South Australia blackout. In this analysis however, we find that it wasn't the dominant cause of the strongest gusts. A major characteristic this feature is that gusts associated with CLs are not continuous and enhanced over many small sections, so some gusts are likely to have been missed by the observation network.

Conclusions

The ETC that brought South Australia to a standstill on the 28th-30th September 2016, contained many characteristics and mesoscale features to those observed in ETCs over western Europe. ETC28 deepened more explosively than all but two over the past 37 years and contained the lowest central pressure as explored in part I of this paper. The widely studied cold-conveyer belt was by far the biggest contributor to extreme gusts; however, convective systems within the dry slot caused a large amount of extremes. The extreme gust causing DSC rarely causes extreme gusts in ETCs over the UK, so warrants further analysis to examine whether this is common extreme gust-producing ETC feature over southern Australian and the Great Australian Bight ETCs. The convective line along the main cold front

was a very violent feature of ETC28 and was responsible for the widely reported South Australia blackout.

Acknowledgements

Parts of this research were made possible by funding from the Australian Research Council (ARC) Grant DP16010997. Nick Earl was also supported by the ARC (CE110001028).

References

Atkins NT, Bouchard CS, Przybylinski RW, Trapp RJ, Schmocker G. 2005. Damaging surface wind mechanisms within the 10 June 2003 Saint Louis bow echo during BAMEX. *Mon. Weather. Rev.*, 133(8): 2275-2296

Baker L. 2009. Sting jets in severe northern European wind storms. *Weather.* 64(6): 143-148.

Browning KA. 2004. The sting at the end of the tail: Damaging winds associated with extratropical cyclones. *Q. J. R. Meteorol. Soc.* 130: 375-399. doi: 10.1256/qj.02.143.

Bureau of Meteorology. 2016. Severe thunderstorm and tornado outbreak South Australia 28 September 2016. 54 pp. http://www.bom.gov.au/announcements/sevwx/sa/Severe_Thunderstorm_and_Tornado_Outbreak_28_September_2016.pdf.

Carlson TN. 1980. Airflow Through Midlatitude Cyclones and the Comma Cloud Pattern. *Mon. Weather. Rev.* 108: 1498–1509.

Carr FH, Millard JP. 1985. A composite study of comma clouds and their association with severe weather over the Great Plains. *Mon. Weather. Rev.* 113: 370–387.

Clark PA, Browning KA, Wang C. 2005. The sting at the end of the tail: Model diagnostics of fine-scale three-dimensional structure of the cloud head. *Q. J. R. Meteorol. Soc.* 131(610): 2263-2292.

Clark MR. 2013. A Provisional Climatology of Cool-Season Convective Lines in the UK. *Atmos. Res.* 123: 180-196.

Cotton WR, Anthes R. 1989. *Storm and Cloud Dynamics.* Academic Press; 883 pp.

Dacre HF, Hawcroft MK, Stringer MA, Hodges KI. 2012. An Extratropical Cyclone Atlas: A Tool for Illustrating Cyclone Structure and Evolution Characteristics. *Bull. Am. Meteorol. Soc.* 93(10): 1497-1502.

Davis C, Atkins N, Bartels D, Bosart L, Coniglio M, Bryan G, Cotton W, Dowell D, Jewett B, Johns R, Jorgensen D. 2004. The bow echo and MCV experiment: Observations and opportunities. *Bull. Am. Meteorol. Soc.* 85: 1075–1093.

Earl N, Dorling S, Starks M, Finch R. 2017. Subsynoptic-scale features associated with extreme surface gusts in UK extratropical cyclone events. *Geophys. Res. Lett.* 44: 3932–3940. doi:10.1002/2017GL073124.

Fink AH, Brücher T, Ermert V, Krüger A, Pinto JG. 2009. The European storm Kyrill in January 2007: synoptic evolution, meteorological impacts and some considerations with respect to climate change. *Natural Hazards and Earth System Sciences*, 9(2): 405-423.

Gray SL, Martínez-Alvarado O, Baker LH, Clark PA. 2011. Conditional symmetric instability in sting-jet storms. *Q. J. R. Meteorol. Soc.* 137(659): 1482-1500.

Hewson TD, Neu U. 2015. Cyclones, windstorms and the IMILAST project, *Tellus A*, 67: 27128.

Keenan TD, Carbone RE. 1992. A preliminary morphology of precipitation systems in tropical northern Australia. *Q. J. R. Meteorol. Soc.* 118(504): 283-326.

Martínez-Alvarado O, Gray SL, Catto JL, Clark PA. 2012. Sting jets in intense winter North-Atlantic windstorms. *Environ. Res. Lett.* 7: 024014.

Neu U, Akperov MG, Bellenbaum N, Benestad R, Blender R, Caballero R, Cocozza A, Dacre HF, Feng Y, Fraedrich K, Grieger J. 2013. IMILAST: A community effort to intercompare extratropical cyclone detection and tracking algorithms. *Bull. Am. Meteorol. Soc.* 94: 529-547. doi: 10.1175/BAMS-D-11-00154.1

Parton G, Dore A, Vaughan G. 2010. A climatology of midtropospheric mesoscale strong wind events as observed by the MST radar, Aberystwyth. *Meteorol. Appl.* 17: 340–354. doi:10.1002/met.203.

Schenkman AD, Xue M. 2016. Bow-echo mesovortices: A review. *Atmos. Res.* 170: 1-13. doi: 10.1016/j.atmosres.2015.11.003

Schultz DM. 2001. Reexamining the cold conveyor belt. *Mon. Weather. Rev.* 129: 2205-2225.

Schultz DM, Browning KA. 2017. What is a sting jet? *Weather.* 72(3): 63-66.

Shapiro MA, Keyser DA. 1990. Fronts, jet streams, and the tropopause. *Extratropical Cyclones: The Erik Palmén Memorial Volume*, C. W. Newton and E. O. Holopainen, Eds. *Am. Meteorol. Soc.* 167–191.

Slater TP, Schultz DM, Vaughan G. 2015. Acceleration of near-surface strong winds in a dry, idealized extratropical cyclone. *Q. J. R. Meteorol. Soc.* 141: 1004–1016. doi:10.1002/qj.2417

Smart DJ, Browning KA. 2014. Attribution of strong winds to a cold conveyor belt and sting jet. *Q. J. R. Meteorol. Soc.* 140: 595–610

Weisman ML. 2001. Bow echoes: A tribute to TT Fujita. *Bull. Am. Meteorol. Soc.* 82(1): 97-116.

Wheatley DM, Trapp RJ, Atkins NT. 2006. Radar and damage analysis of severe bow echoes observed during BAMEX. *Mon. Weather Rev.* 134(3): 791-806.

Feature	5%	1%	0.1%
CCB	46	33	8
CC	12	1	0
DSC	11	6	4
CL	8	5	3
Pseudo-CL	7	7	2
DCB	3	3	0
Strong PG	3	0	0
WCB	1	0	0

Table 1 – Total number of DMGSs of all the contributing features during the passage of ETC28 for the three thresholds.

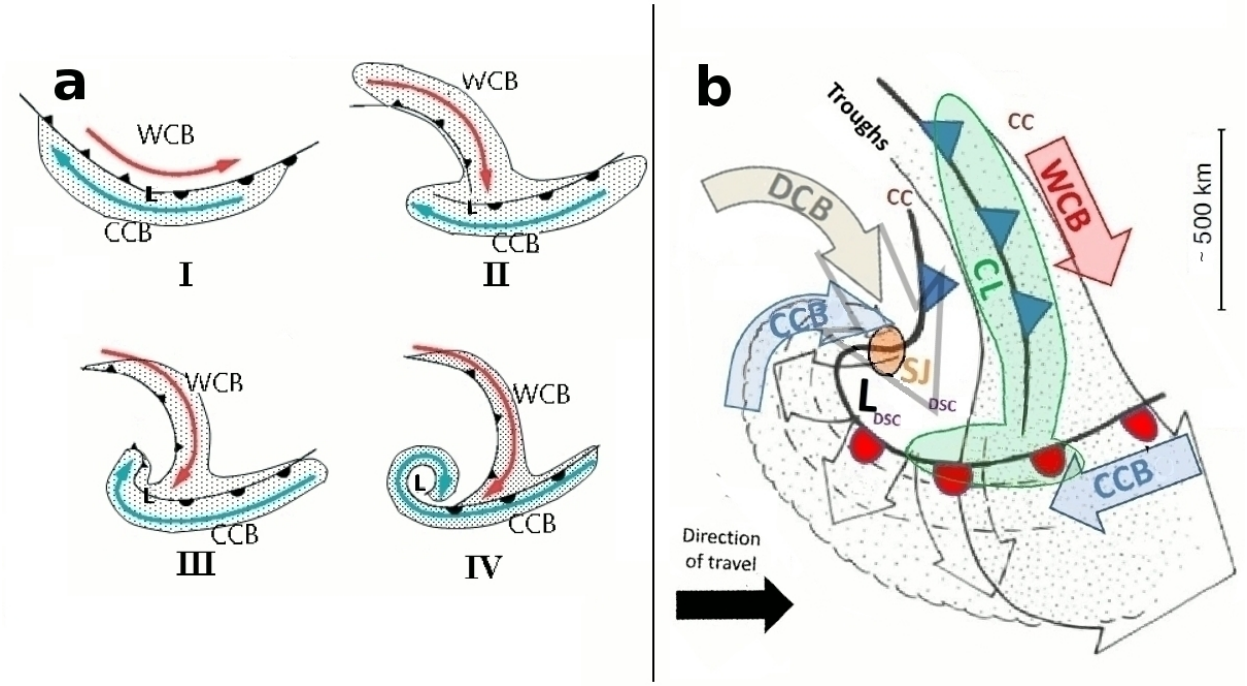

Figure 1. a. Shapiro-Keyser conceptual model of the life cycle of an extra-tropical cyclone: (I) open wave, (II) frontal fracture, (III) bent-back front and frontal T-bone, and (IV) mature, frontal seclusion (adapted for the southern hemisphere). The cold and warm conveyor belts (CCB and WCB respectively) are marked along with the low pressure centre (L) and the cloud signature (stippled areas) (adapted from Baker, 2009). b. Conceptual model of sub-synoptic-scale features within an extra-tropical cyclone, during transition from stage III to stage IV (adapted from Browning, 2004, for the southern hemisphere). Also displays where convective system (CC), dry slot convection (DSC), dry conveyor belt (DCB), convective line (CL) and sting jet (SJ) associated gusts can occur in relation to the cyclone.

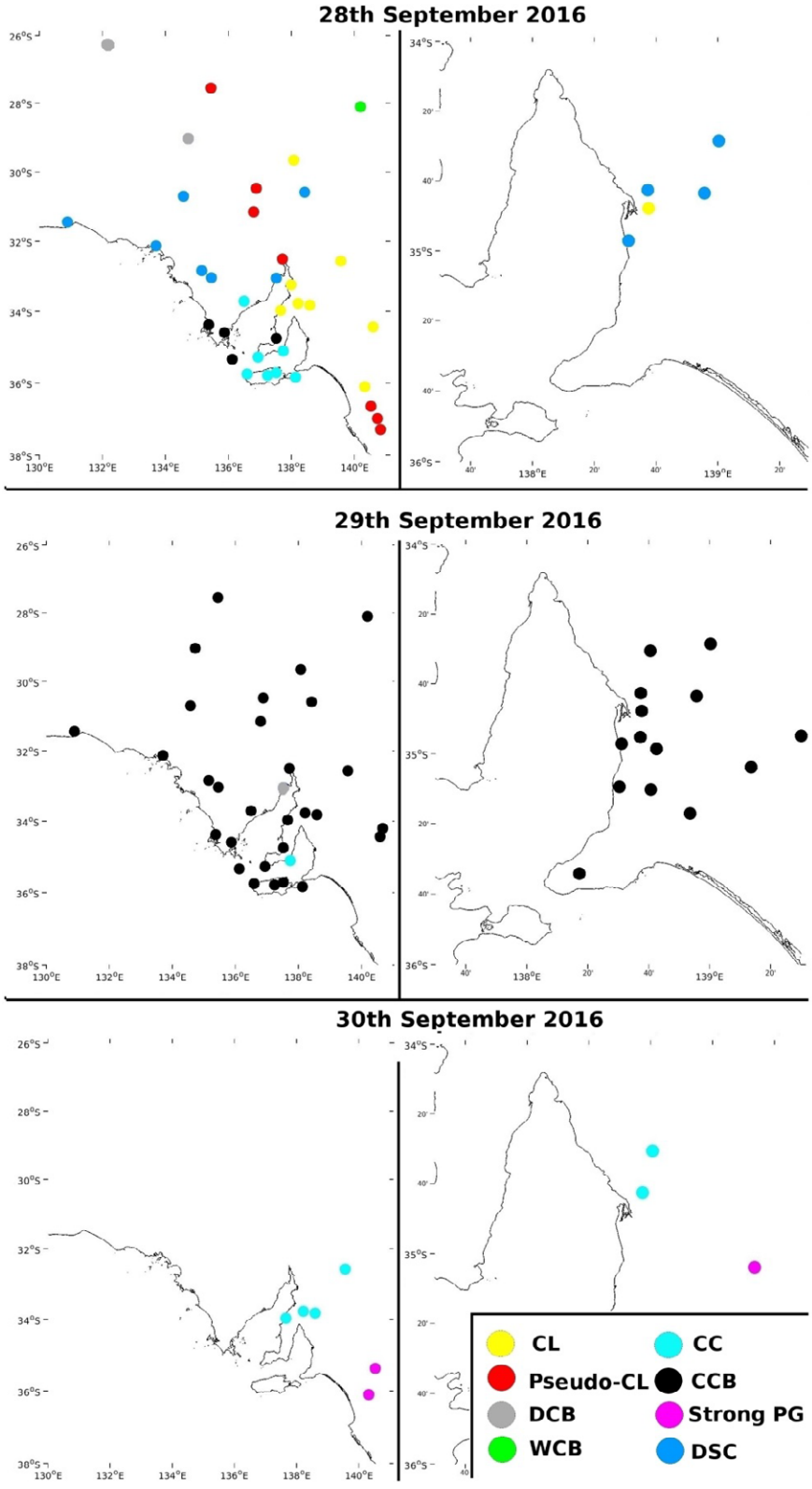

Figure 2. Location of gust and associated feature for the top 5% of DMGSs affecting the surface on the 28th, 29th and 30th September 2016. The whole of South Australia is displayed on the left panels and the Adelaide area on the right panels for clarity.

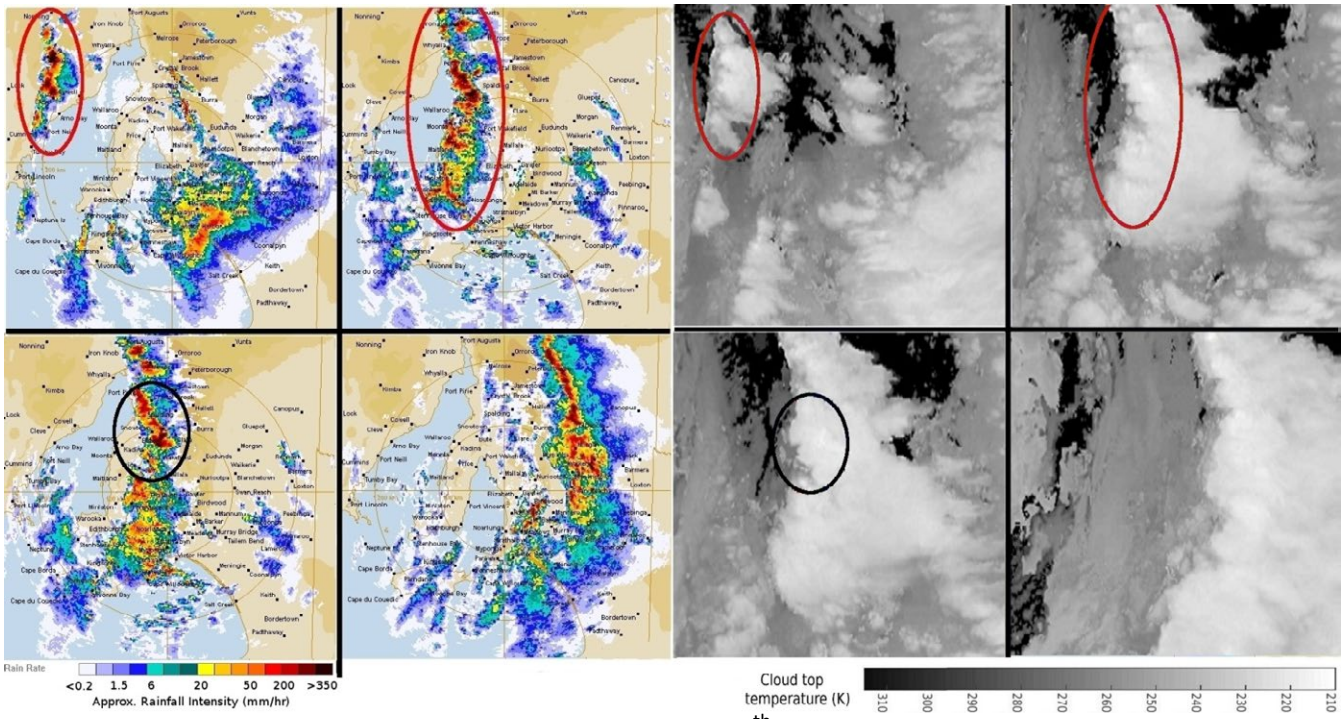

Figure 3 – Radar and satellite infrared images from the 28th September 2016 at 13:20 ACST (top left) 15:00ACST (top right), 15:20ACST (bottom left) and 17:20ACST (bottom right). The red ovals show the CL development and black highlight the bow shape causing the intense gust at Snowtown.

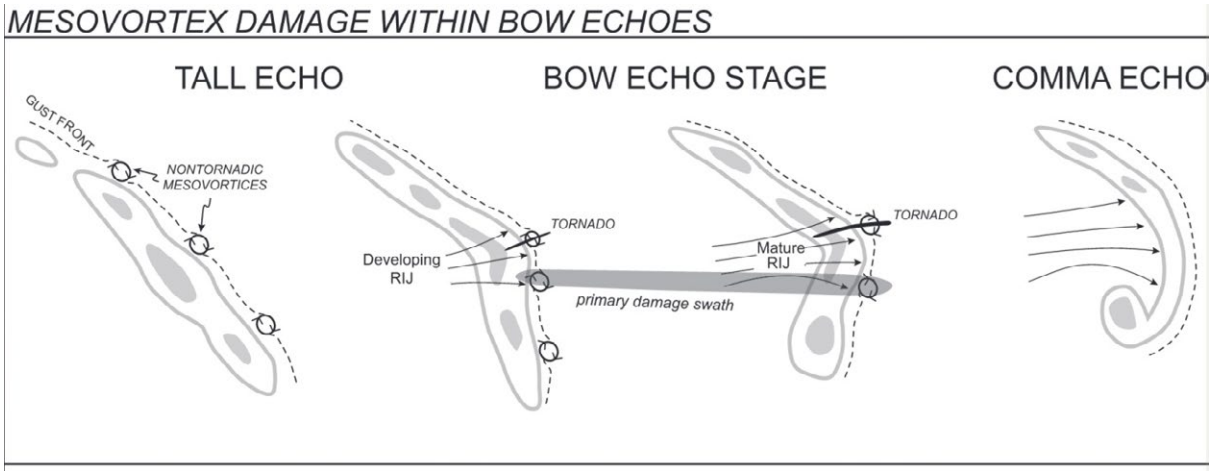

Figure 4 – Schematic diagram of a bow echo and attendant damage produced by mesovortices adapted (from Atkins *et al.*, 2005) for the southern hemisphere.

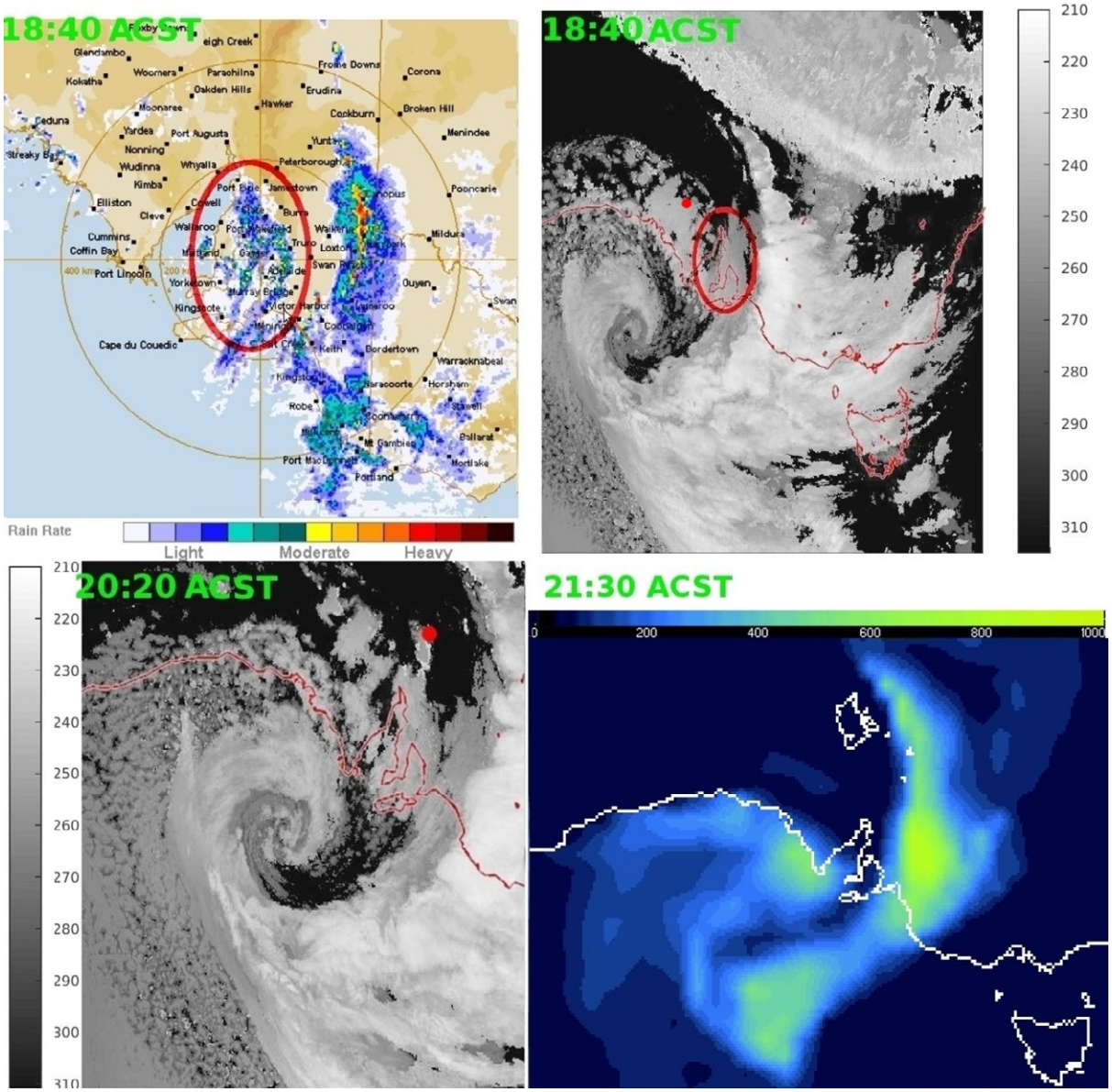

Figure 5 – Radar (rainfall rate) and infrared (cloud to temperature in Kelvin) highlighting DSC over the Adelaide Metrapolitan area at 18:40 ACST on the 28th September 2016 and infrared image displaying the cell at Leigh Creek (red dot) at 20:20 ACST (DMGS at Leigh Creek occurred at 20:19 ACST). The red dot in the 18:40 ACST infrared image displays the location of the DSC which later affected Leigh Creek. Also displayed is the convectively available potential energy (CAPE) from ERA-interim (J kg^{-1}) 12 hour forecast for 21:30 ACST.

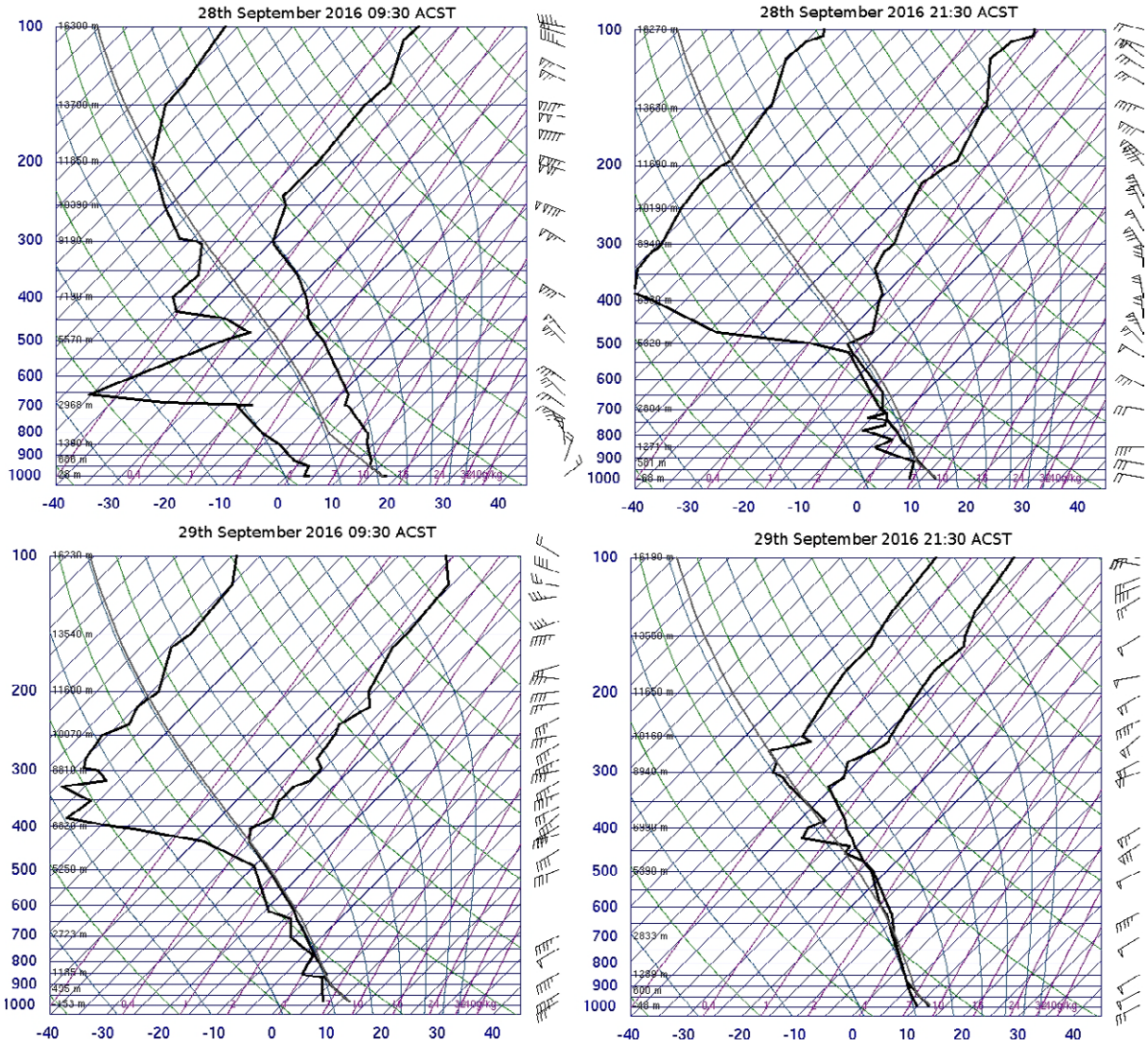

Figure 6 – Atmospheric soundings from Adelaide Airport on the 28th and 29th September 2016 from the University of Wyoming (available from http://weather.uwyo.edu/upperair/sounding.html). Right hand lines represent temperature and left dew point temperature in degrees Celsius. Wind barbs follow standard notation (small barb - 5 Knots, long barb – 10 Knots, triangle – 50 Knots and directions from where the wind is coming).

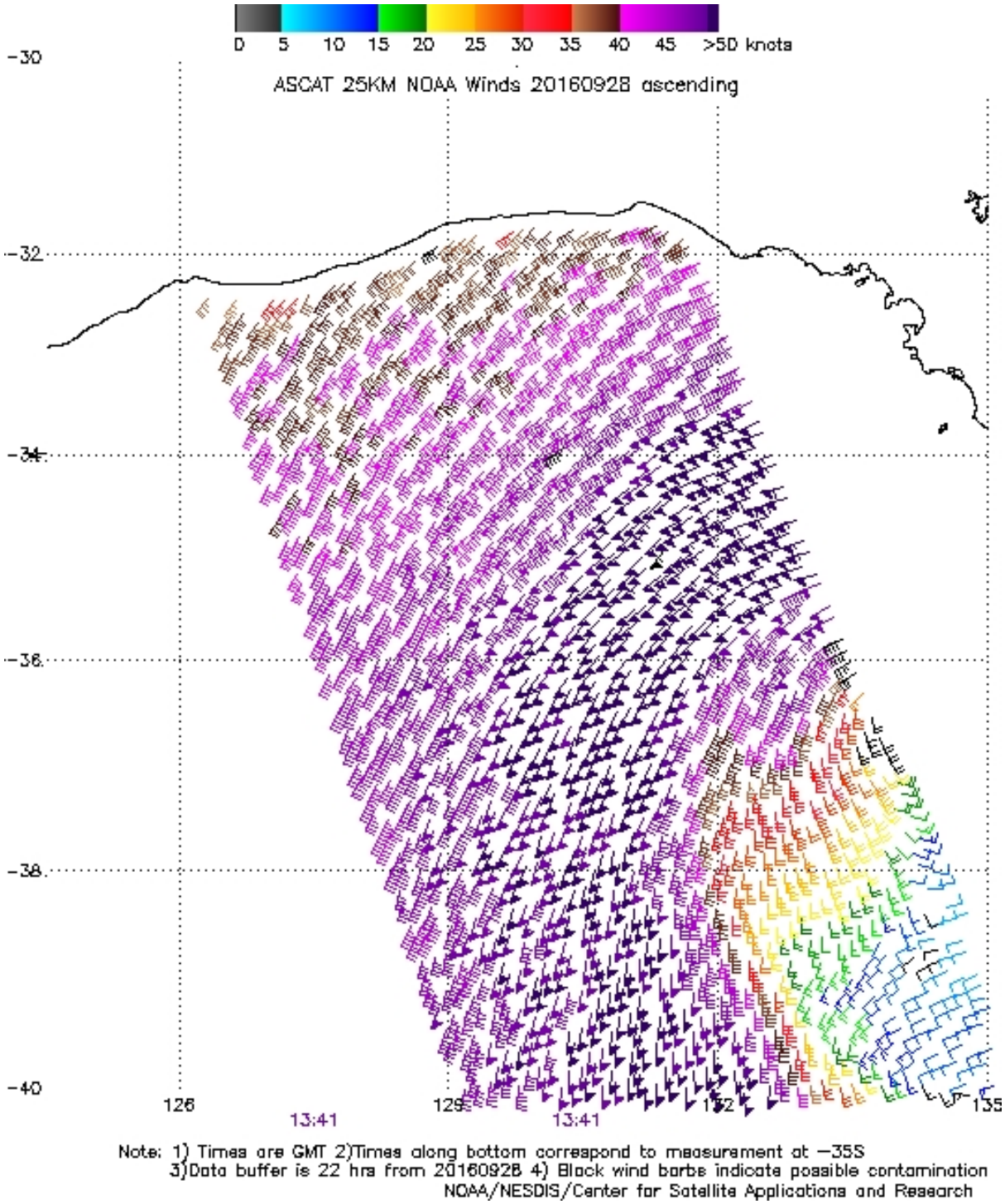

Figure 7 – ASCAT scatterometer (from https://manati.star.nesdis.noaa.gov/datasets/ASCATData.php) highlighting the extent of the CCB winds over the Bight at 23:11 ACST (13:41 UTC) on the 28th September

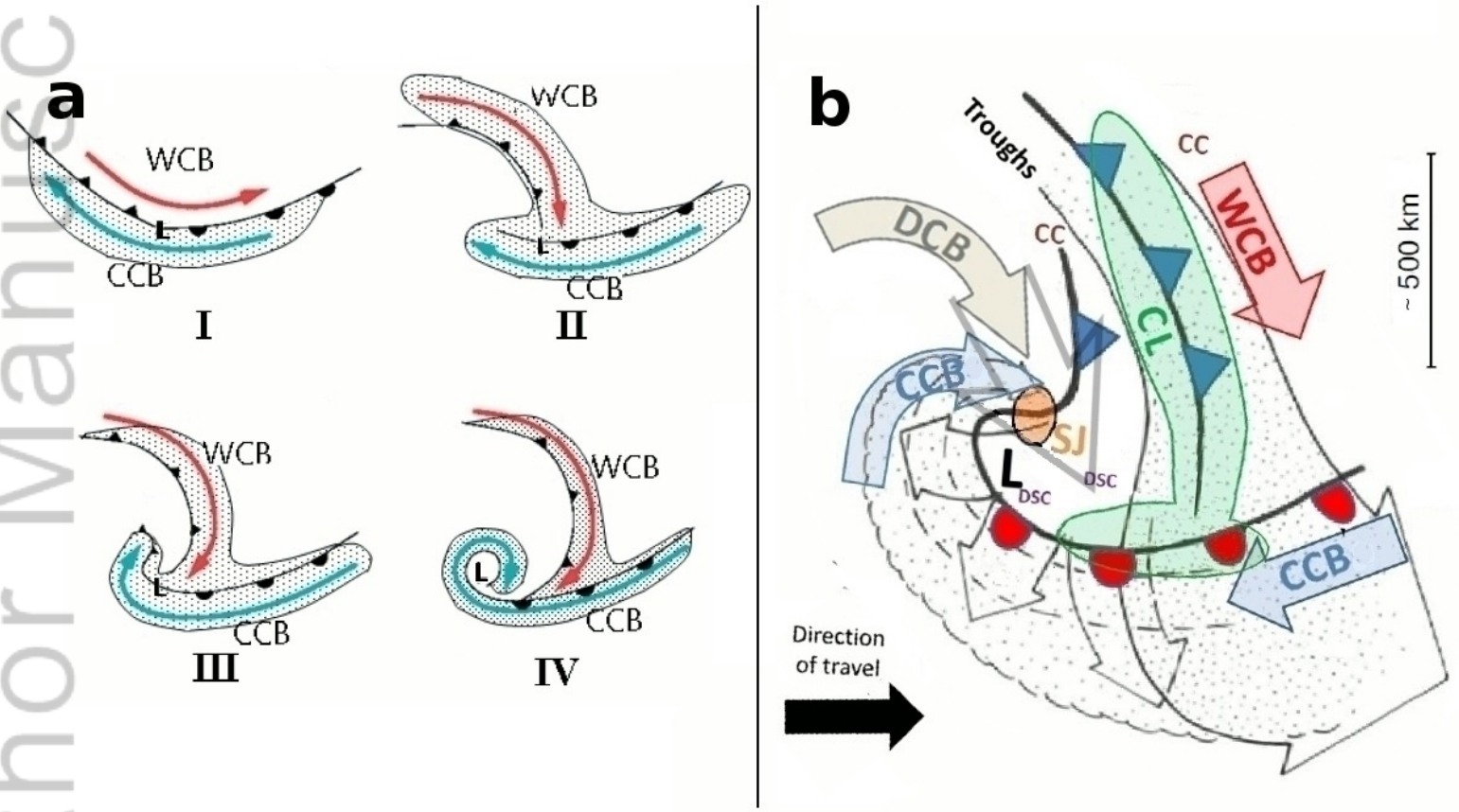

Fig1.jpeg

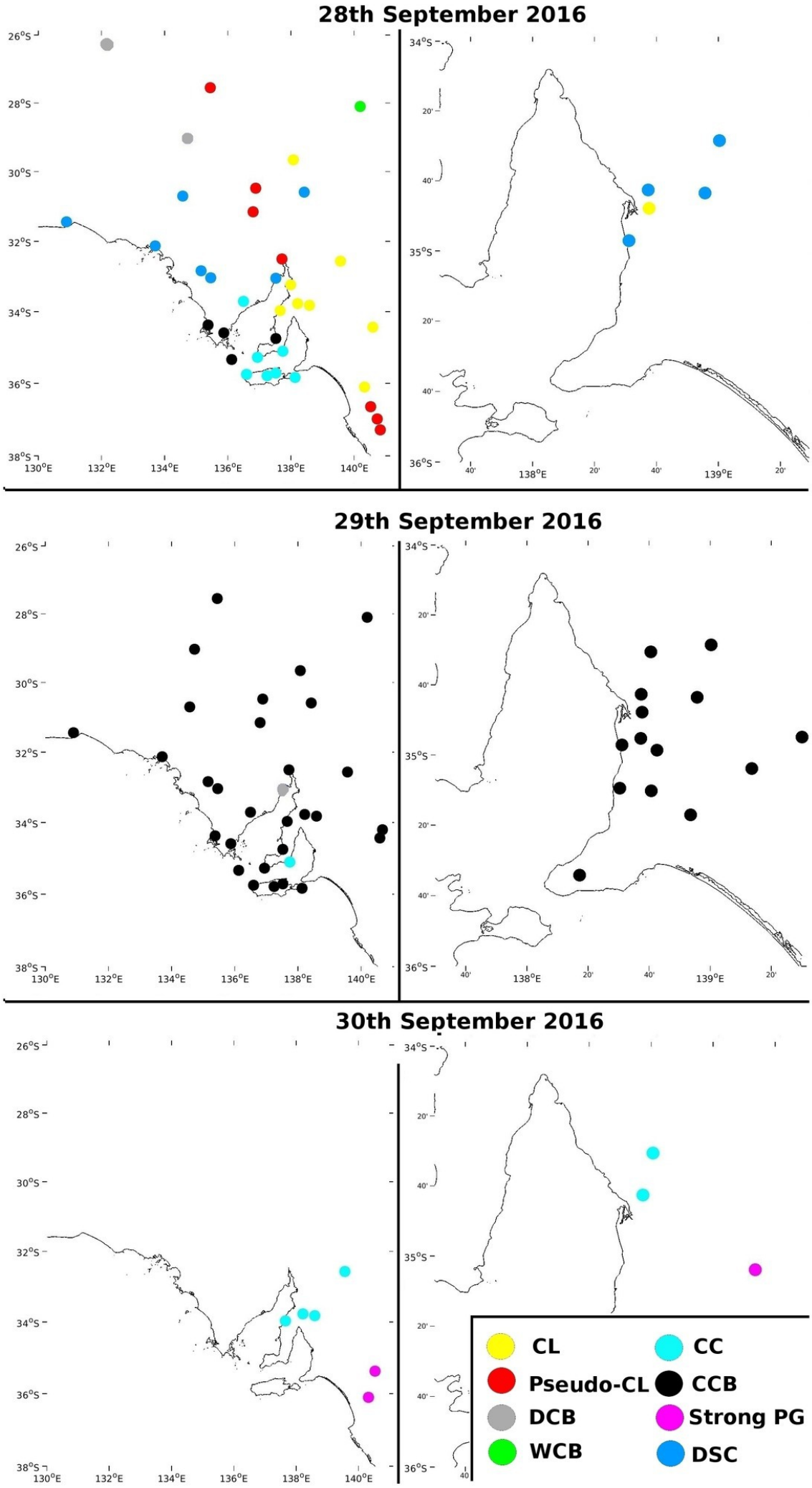

Fig2.jpeg

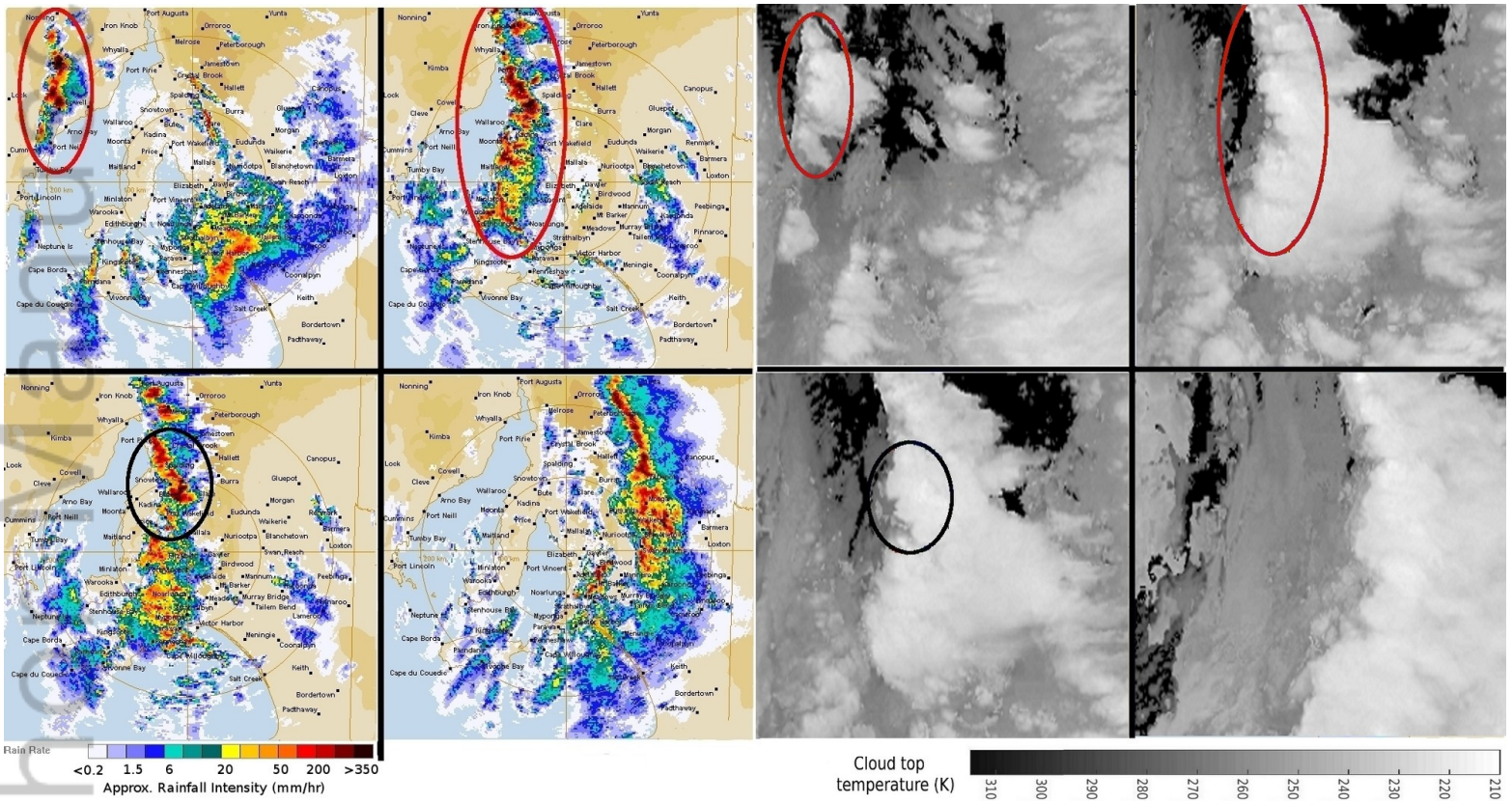

Fig3.jpeg

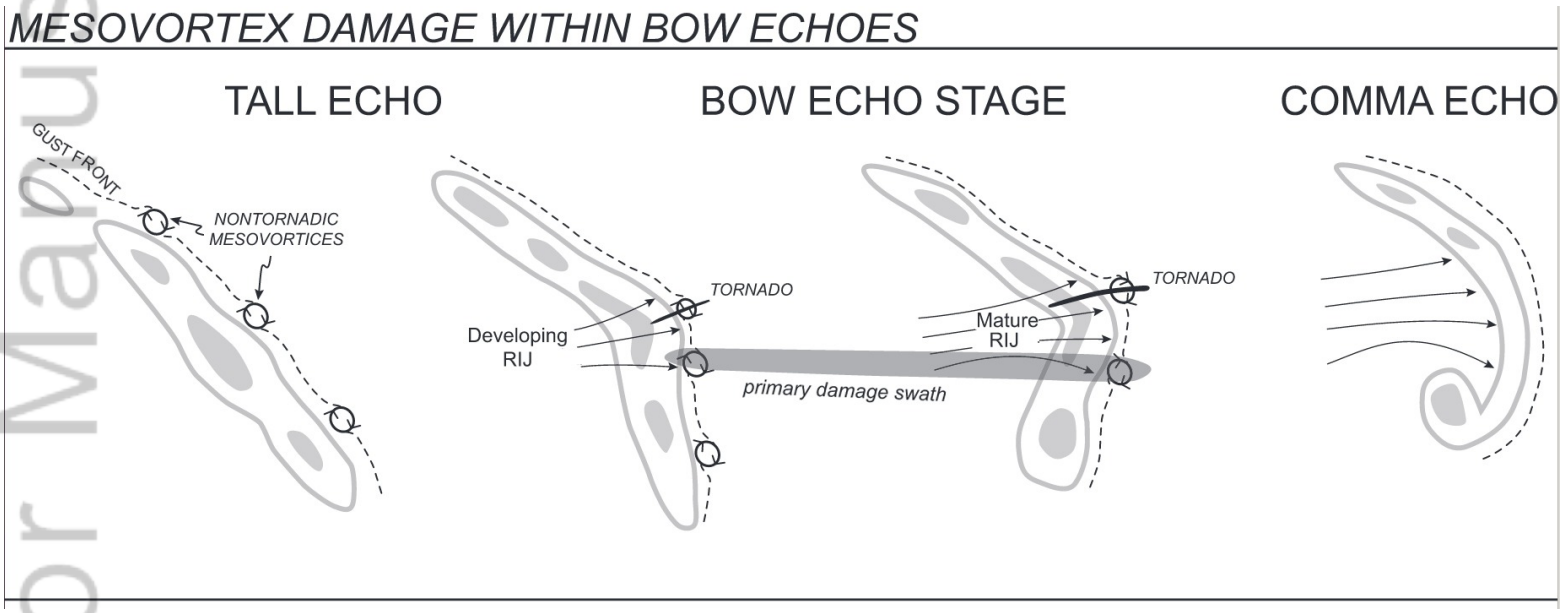

Fig4.jpeg

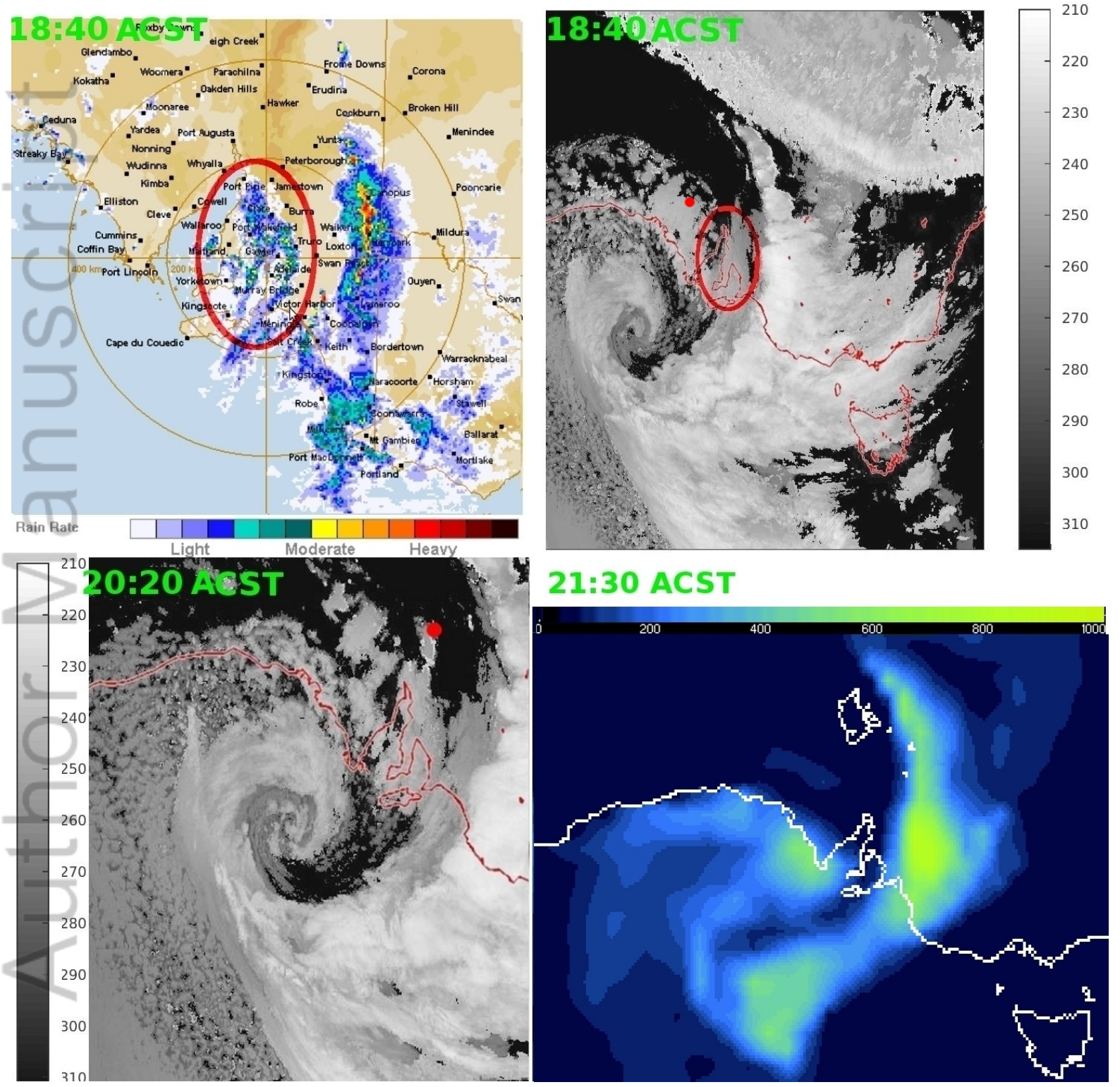

Fig5.jpeg

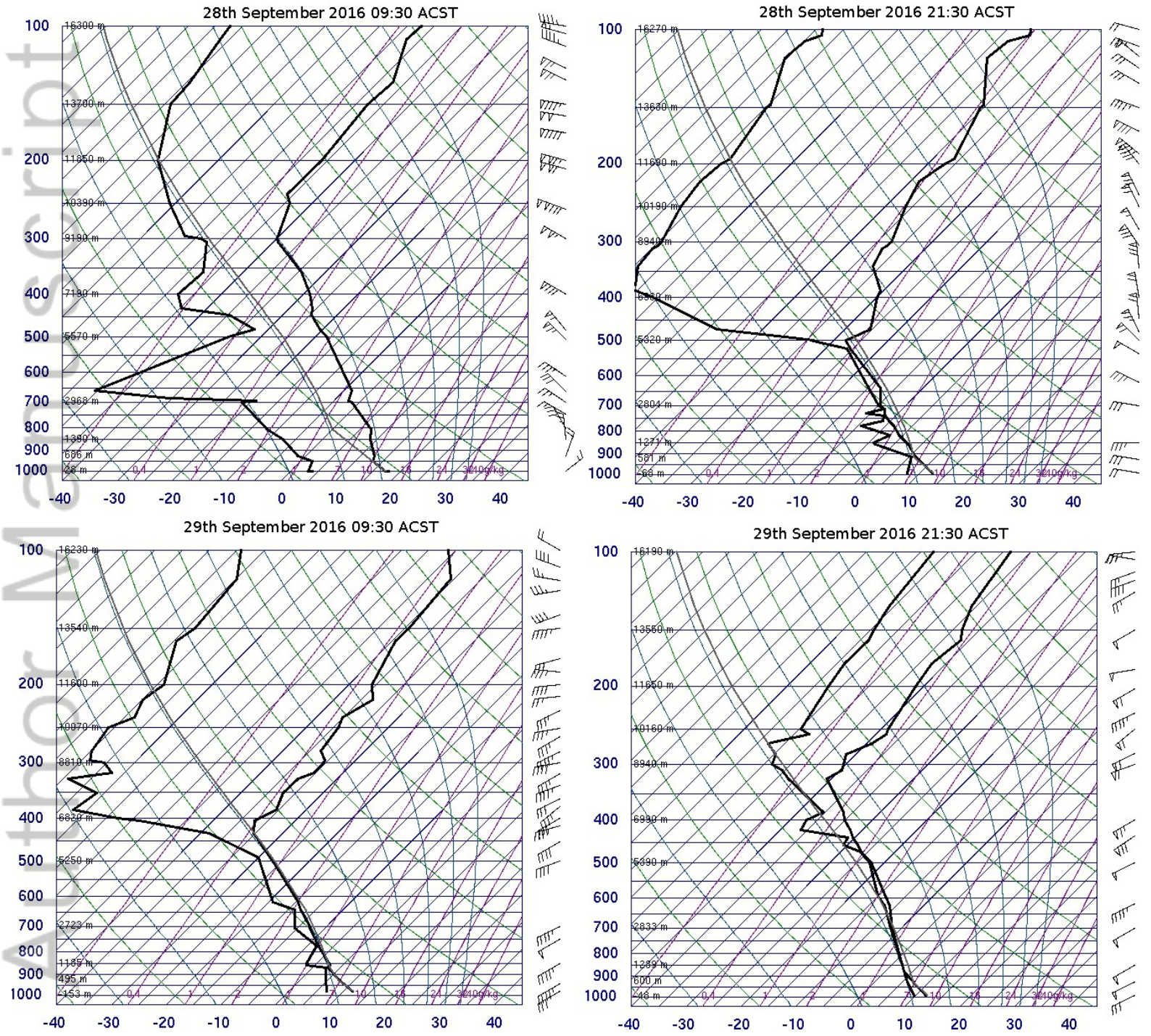

Fig6.jpeg

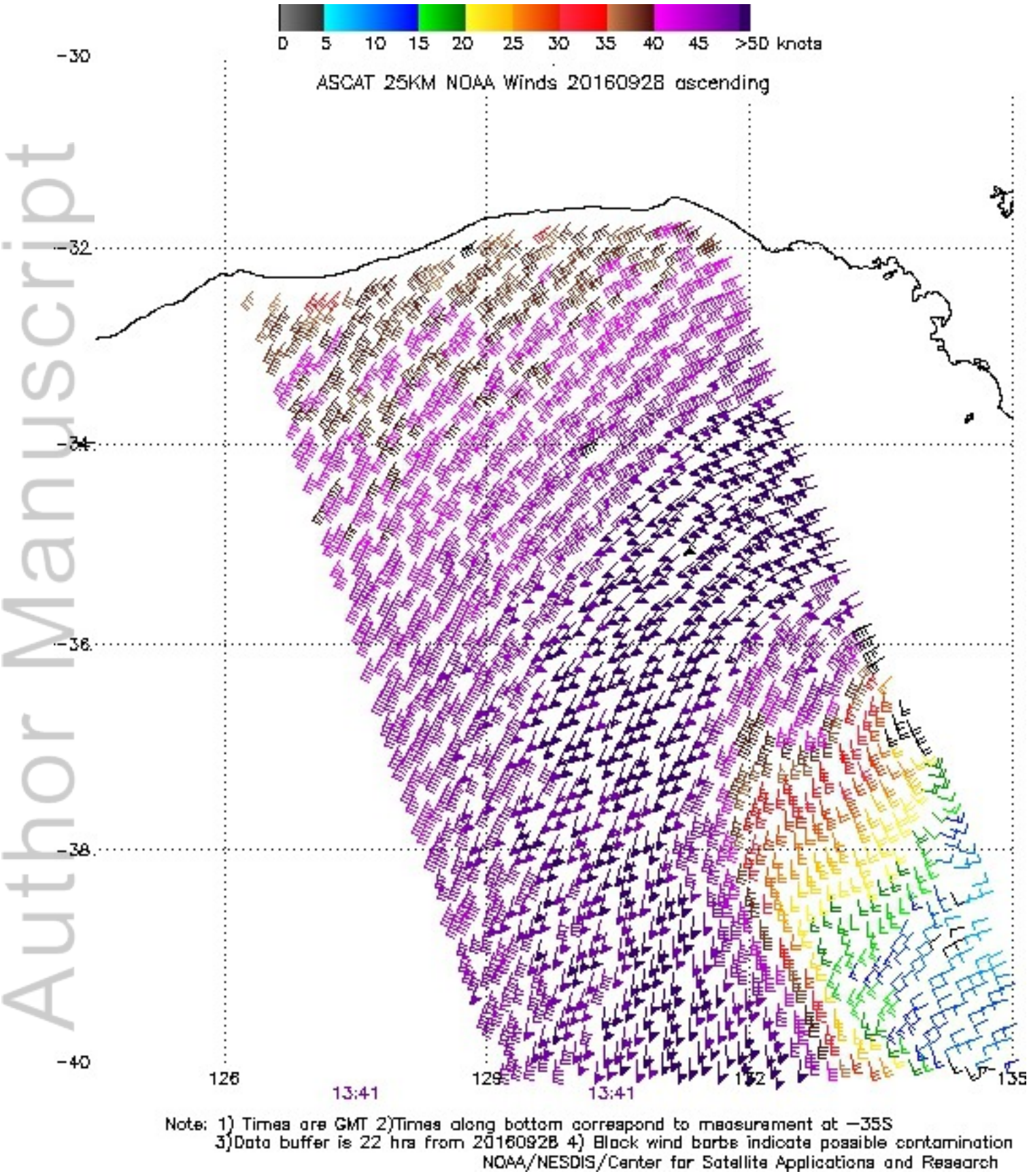

Fig7.jpeg

Dear Dr. Earl,

Your manuscript has been reviewed and the comments of the reviewers may be found at the foot of this message. They have recommended publication after some revisions have been made. Accordingly, I invite you to respond to the comments and revise your manuscript.

You have 90 days to submit your revised paper, after which the online submission system will block its upload. If you need more time please contact weather@wiley.com. However, it would be much appreciated if your revision could reach us well before the 90 days are up.

You can upload your revised manuscript and submit it through your Author Centre. Log into https://protect-au.mimecast.com/s/GmYYCq7By5s2GyKJFZoto3?domain=mc.manuscriptcentral.com and enter your Author Centre, where you will find your manuscript title listed under "Manuscripts with Decisions".

When submitting your revised manuscript, you will be able to respond to the comments made by the reviewers in the space provided. You can use this space to document the changes you make to the original manuscript.

IMPORTANT: Please make sure you closely follow the instructions for acceptable files. When uploading your revised manuscript, please delete the file(s) that you wish to replace and then upload the revised file(s).

Once again, thank you for submitting your manuscript to Weather. I look forward to receiving your revision.

Yours sincerely,

Mr. James Galvin

rmetseditorialoffice@wiley.com

Dear Jim,

Thank you again for overseeing our submissions. Based on the comments made by the reviewers we have fine-tuned the manuscript as indicated below.

Review: 1

Comments to the Author

Thank you again, a good read of a worthwhile subject. I hope it leads to the further suggested research.

Your research and conclusions are remarkably detailed.

Again, I have some recommendations for minor changes to the paper, listed below.

We thank the reviewer again for positive views and helpful comments and have addressed each of them below.

Figure 2 is a duplicate of Part I's figure 3, but the only version with the annotations referred to within the text. (From the Editor: please change Fig. 3 of Part 1 to include annotations and refer back to it from this part, rather than include it.)

Thanks for making this point. Our thought was to include a more detailed version of Figure 3 Part I here as we refer to it a great deal in part II. We, however, understand the point that is being made here. In light of this we have removed the Figure from the present Part II, and have placed the detailed version in Part I.

Line no. (pdf version line numbers)

73 replace ...when aligned with... with ...in the direction of...

Thanks, this has been adjusted.

93 sp. z vs s

Thanks, we have now used the English spelling

120 'different to' rather than 'dissimilar from'

Your suggestion is much better than our original choice of words. These have now been included.

192 'as low as the front's' rather than 'as cold as the fronts'

Thanks, we have made this suggested change.

195 'lower' rather than 'cooler'

Thanks again.

215 'higher' rather than 'warmer'

Thanks for pointing out the more appropriate terminology here.

253 knots, or ms-1?

It's knots for this scatterometer

Review: 2

Comments to the Author

Similar comments to part 1 really. Well written and relevant to Weather readers.

Many thanks again for your efforts with these manuscripts.

Introduction

"In part 1 of this paper..." This will need a reference when available.

OK yes, thanks

There a few minor spelling or syntax errors, i.e. under convective Line - "forsimplicity" ?

OK thanks for pointing this out.